Detrital remanent magnetization in the solar nebula

Roger R. Fu[1] and Benjamin P. Weiss[1]

Received 10 August 2011; revised 28 November 2011; accepted 29 November 2011; published 9 February 2012.

[1] We introduce the theoretical basis of a new form of remanent magnetization that likely formed on primitive bodies in the solar system. Accretional detrital remanent magnetization (ADRM) operates via "compass needle"-type alignment of ferromagnetic solids with locally uniform background fields in the solar nebula. Accretion of coherently aligned magnetic particles should have formed aggregates up to centimeters in size with significant net magnetic moment. We quantify several processes that constrain the likelihood of ADRM formation, finding that rotational gas damping and background field intensities expected for the solar nebula are sufficient to mutually align magnetic particles with diameters between ~30 μm and several cm. The lower bound is dictated by Brownian motion or radiative torque while the upper bound is set by aerodynamic torque on non-spherical particles. Processes important for interstellar dust dynamics such as Larmor-type precession and Purcell torque are less significant in the solar nebula. ADRM can be potentially observed as zones of coherent magnetization in primitive chondrites and may be detected by spacecraft magnetic field observations on the surfaces of small bodies. Observational identification and characterization of ADRM would constrain the strength and geometry of magnetic fields in the early solar system, the accretion process of sub-meter sized objects, the formation regions of chondrite parent bodies, and the alteration history of chondritic components.

Citation: Fu, R. R., and B. P. Weiss (2012), Detrital remanent magnetization in the solar nebula, *J. Geophys. Res.*, *117*, E02003, doi:10.1029/2011JE003925.

1. Introduction

[2] Remanent magnetization in primitive materials provides one of the few direct records of magnetic fields present during the accretion stage of the solar system. Magnetic fields coupled to conducting nebular gas have been proposed as the principle mechanism responsible for outward angular momentum transport and inward mass transport in the accretion disk [e.g., *Balbus and Hawley*, 2000]. In this process, known as the magnetorotational instability (MRI), infalling material in the accretion disk is weakly coupled to material at greater orbital radii via magnetic fields in the 10 to 100 μT range. The nebular field therefore may have played a key role in establishing the large scale radial mass distribution in the solar system. Heating events associated with reconnection of nebular fields may have also formed chondrules and melted calcium-aluminum-rich inclusions (CAIs), the lithic constituents of chondritic meteorites [*Levy and Araki*, 1989; *Joung et al.*, 2004]. However, reliable direct constraints on the strength and morphologies of solar nebular magnetic fields have proven elusive, and the precise role of magnetic fields in the accretion process remains uncertain.

[3] At the same time, the process of growth for particles between 1 cm and 1 km in size in the solar nebula remains an open question. Unlike smaller particles, which efficiently form agglomerates during mutual collisions, particles at the centimeter scale or larger may undergo non-sticking collisions [e.g., *Paraskov et al.*, 2007; *Zsom et al.*, 2010]. As a result, several competing hypotheses exist to facilitate the accretion of such particles into kilometer-sized planetesimals, at which size gravitational attraction accelerates the accretion process [e.g., *Johansen et al.*, 2007; *Cuzzi et al.*, 2008].

[4] Remanent magnetism in primitive solar system materials could provide records of the magnetic fields in the early solar system. It may also constrain the nature and timing of early remagnetization events such as thermal metamorphism and aqueous alteration in the nebular environment and on planetesimals [*Weiss et al.*, 2010]. In the latter case, remanence acquired on primitive parent bodies may record fields generated by interior metallic core dynamos, thereby constraining the timing and extent early planetesimal accretion and differentiation [*Carporzen et al.*, 2011]. Furthermore, relationships between the magnetization of different components in meteorites (e.g., between chondrules or between chondrules and matrix) can potentially distinguish amongst the various proposed accretional processes.

[5] Records of ancient fields have been observed in meteorites and possibly via spacecraft flybys of primitive bodies [e.g., *Weiss et al.*, 2010, 2008; *Richter et al.*, 2001]. Most such remanence has been identified as thermoremanent magnetization (TRM) or crystallization remanent magnetization (CRM) that formed during thermal and crystallization

[1]Department of Earth, Atmospheric and Planetary Sciences, Massachusetts Institute of Technology, Cambridge, Massachusetts, USA.

0148-0227/12/2011JE003925

events in the nebula or following accretion on planetesimals. However, during accretion, there are at least two additional ways by which ferromagnetic particles may form magnetized materials at larger scales.

[6] Firstly, strongly ferromagnetic particles with sizes of ~10 nm may accrete as a result of their mutual magnetic attraction, thereby forming chain-like structures with increasingly larger net magnetic moments. This possibility, which we refer to as accretional attractive remanent magnetization (AARM), was addressed in detail by several numerical [*Nübold and Glassmeier*, 2000; *Dominik and Nübold*, 2002] and laboratory studies [*Nübold et al.*, 2003; *Wang et al.*, 2010]. These studies found that AARM acting upon Fe metal and magnetite-rich particles with strong magnetizations can form "fluffy" aggregates of low fractal dimensions with sizes ranging from 0.1 μm to 1 mm. Beyond this limit, the specific moment of the aggregates becomes insufficient for the particles' mutual magnetic attraction to be the dominant factor in further aggregation. AARM may therefore have played an important role in the formation of the first macroscopic grain aggregates in the solar nebula.

[7] AARM is not the focus of the present study. Rather, we describe a second process whereby both weakly and strongly ferromagnetic particles accreting in a background magnetic field may become mutually aligned to produce even larger structures with significant net magnetic moment. Unlike in AARM, the magnetic field in the latter process is ambient (i.e., is not generated by the particles themselves) and serves to align the grains rather than act as an attractive force that enhances accretion (such that other forces like gravity and electrostatic attraction are relied upon for accretion). On Earth, the effect of such a process is ubiquitously observed in sedimentary rocks and is termed detrital remanent magnetization (DRM). Here we show how an analogous process that we call accretional detrital remanent magnetization (ADRM) should have operated during the accretional phase of the solar nebula. We also demonstrate that ADRM may be preserved in primitive meteorites, interplanetary dust particles (IDPs), asteroids, and comets. As described below, it may even have already been observed in some chondritic meteorites. Identification and characterization of ADRM may yield new constraints about the magnetic and dynamic environment of the early solar system as well as the accretion process of solid particles.

[8] In ADRM, ferromagnetic grains are aligned such that their magnetic dipole moment is parallel to the background field. Such a "compass needle" alignment mechanism was also proposed as an explanation for the polarization of light passing through interstellar dust aligned to the interstellar magnetic field [*Spitzer and Tukey*, 1951]. This mechanism has since been shown to be implausible in the interstellar medium (ISM) given the weak intensity (~0.3 to 0.4 nT) of interstellar fields [*Draine and Weingartner*, 1997]. Instead, most observed grain alignment in the ISM is likely caused by a combination of radiative torque due to impinging light and paramagnetic dissipation. In the latter process, also known as the Davis-Greenstein effect, the rotation axis of rapidly spinning grains align to the ambient magnetic field over timescales of up to 10^6 yr. Other alignment mechanisms, such as interaction with interstellar gas flow fields, have also been proposed [*Gold*, 1952].

[9] However, as shown in section 2, several conditions should have favored compass needle alignment over these other mechanisms for ferromagnetic particles in the solar nebula. Firstly, observations of chondrites indicate there should have been significant quantities of highly ferromagnetic material present in the nebula. Magnetic minerals including magnetite, pyrrhotite, and Fe-Ni metals are present in both meteorite components such as CAIs and chondrules [*Zolensky et al.*, 2006]. FeNi metals and sulfides have also been identified in cometary grains and glassy pre-solar inclusions in interplanetary dust particles (IDP) [*Bradley*, 1994; *Nakamura et al.*, 2008]. Secondly, the much denser gas medium of the nebula (by a factor of $\sim 10^9$ relative to that of the ISM) causes rapid decay of angular velocity on a timescale far shorter than that of the Davis-Greenstein effect. Thirdly, the magnetic fields in protoplanetary disks are expected to be more than 10^3 times stronger than those of the ISM: direct observations of star-forming regions suggest that the ambient magnetic field in a protoplanetary disk is ≥ 1 μT [*Wardle*, 2007]. Finally, the larger particle sizes in the solar nebula relative to the ISM reduce the relative importance of processes that lead to rapid rotation of particles such as radiative torque, which has been proposed to operate only on small particles (<100 μm) in the outer portions (10–100 AU) of T Tauri disks [*Cho and Lazarian*, 2007].

[10] Ferromagnetic particles will align with the background field when 1) the timescale of magnetic alignment is short compared to that of periodic, disruptive processes and 2) the dominant torque on the particle is magnetic. In section 2, we describe a set of models used to constrain the range of particles and locations in the disk where alignment to a background field is expected. These models address eight distinct processes that affect the orientations of magnetic particle in the solar nebula:

[11] 1. mutual collisions between dust grains

[12] 2. rotational gas drag

[13] 3. Larmor-type precession around the background field direction

[14] 4. rotational Brownian motion

[15] 5. aerodynamic torque on non-spherical grains

[16] 6. accommodation torque due to variations in momentum transfer efficiency on grain surface during gas molecule collisions

[17] 7. radiative torque on irregular grains

[18] 8. Purcell torque due to H_2 formation at enhanced surface sites.

[19] We quantify the effect of each of these processes and evaluate the likelihood of ferromagnetic grain alignment and formation of ADRM over a range of particle and nebula parameters. The results of our models are presented in section 3.

[20] In section 4, we qualitatively address other relevant processes. We first use the results of recent dust collision experiments to identify the classes of collisions that would lead to the preservation of grain alignment in accreting dust agglomerates. We then discuss and evaluate the degradational effects of post-accretional impacts and parent body alteration processes of ADRM. The requirements on temporal and spatial uniformity of the background field are outlined. We identify several observations from past chondrite paleomagnetism that may be attributed to ADRM. Finally, we discuss the possibilities for future observations

Table 1. Definition of Selected Variables and Constants Used in This Work in Order of Appearance

Symbol	Meaning	Value
T_{gas}	Nebular gas temperature	Var.
R	Orbital radius	Var.
ρ_{gas}	Nebular gas mass density	Var.
t_{coll}	Mean time between solid particle collisions	Var.
σ	Cross-sectional area of solid particle	Var.
n	Number density of solid particles in nebula	Var.
v_{rel}	Relative velocity among particles to find t_{coll}	Var.
r_p	Solid particle radius	Var.
ρ_p	Individual particle density	2000 kg m^{-3}
ρ_s	Mass density of solids in nebula	Var.
t_f	Timescale of $1/e$ decay in velocity	Var.
ω	Particle angular velocity	Var.
τ_{FM}	Gas drag torque in FM regime	Var.
τ_{LR}	Gas drag torque in LR regime	Var.
τ_B	Magnetic torque	Var.
f	Momentum transfer coefficient for FM rotational drag	1
$\bar{c}$	Mean gas molecule velocity in center of mass frame	Var.
I	Moment of inertia of a uniform sphere	Var.
t_{FM}	Timescale of $1/e$ decay of ω in FM regime	Var.
t_{LR}	Timescale of $1/e$ decay of ω in LR regime	Var.
t_{drag}	Shorthand for t_{FM} or t_{LR} as appropriate	Var.
θ	Angle between magnetic field and particle moment	Var.
j	Specific magnetic moment of particle	10^{-5} Am^2 kg^{-1}
B_{FM}	Field strength for critical damping in FM regime	Var.
B_{LR}	Field strength for critical damping in LR regime	Var.
t_{prec}	Timescale of sufficient decay in ω to allow alignment	Var.
t_{align}	Total time necessary for magnetic alignment	Var.
θ_{crit}	Maximum tolerance for θ of "aligned" particle	$\pi/10$
χ	Aspect ratio of prolate ellipsoid particle	1.1 and 2

and their potential implications for our understanding of the early solar system.

2. Model Descriptions

2.1. Overview

[21] Before delving into the physics of grain alignment, we provide a qualitative overview of the processes involved. In the solar nebula, solid particles composed of rock, ice, and metals with sizes ranging from 1 μm to many meters orbited the sun embedded in a tenuous gas environment ($\sim 10^7$ times less dense than air at sea level, but still $\sim 10^{14}$ times denser than interstellar space). Many of these particles should have contained ferromagnetic grains, which should have experienced a torque that could lead to alignment with the local magnetic field. For magnetic alignment to be successful, it must proceed more rapidly than the timescale of mutual collisions between solid particles, which disrupt alignment by imparting random, fast angular velocities to the grains (section 2.3). Rapidly spinning grains lose their angular velocity due to gas drag (section 2.4). If a grain spins down quickly before the occurrence of the next interparticle collision, it is free to align to the local magnetic field in the absence of another, stronger torque acting on the grain (section 2.5). These other possible effects include thermal excitation, aerodynamic torque, radiative torque, and several other processes (sections 2.6–2.11).

[22] If the conditions are satisfied such that grains align to the local magnetic field, further agglomeration of these coherently aligned particles may form a net magnetic moment pointing in the direction of the local magnetic field. The net moment of the agglomerate grows until it reaches a regime where the agglomerate's orientation is no longer controlled by magnetic torques. The accretion of small, magnetically aligned agglomerates onto a nascent planetesimal, perhaps due to a local dynamical instability, may form large regions of uniform magnetization (sections 4.2 and 4.3).

2.2. The Solar Nebula

[23] We begin with a brief description the of the solar nebula environment. Although there is uncertainty regarding the evolution of the nebula during the time of planet formation, it is likely that the accretion of sub-micrometer dust particles into kilometer-sized planetesimals took place over a timescale of order one million years [*Weidenschilling and Cuzzi*, 2006]. Most workers assume that the total initial mass of solid particles is equal to the combined mass of solids in the present-day solar system disk and that the total initial mass of gas is greater than that of solids according to the observed solar relative abundances. A disk with this assumed property is known as the minimum mass solar nebula (MMSN). The initial distribution of both gas and dust is expected to be in a flared disk up to 50 AU in radius. With time, solid particles settle to the midplane, creating a dust sub-layer whose height is determined by the amount of turbulence in the gas, which acts to suspend solid particles away from the disk midplane.

[24] Due to the radial pressure gradient in the disk, gas molecules experience a slightly smaller centripetal acceleration than dust particles at the same location and therefore orbit more slowly. Larger dust particles are less coupled to the gas and feel a stronger "headwind." This effect, in conjunction with turbulent gas motion, generates relative velocities between dust particles, allowing them to collide and accrete. Such "hit and stick" agglomeration is an efficient method of forming particles of up to several centimeters in size [*Zsom et al.*, 2010] in the standard MMSN and may be an important factor in accretional growth at even larger sizes. Growth by mutual collisions may be aided by local enhancements of density, leading to gravitational instabilities that form km-size planetesimals [*Cuzzi et al.*, 2008]. These objects in turn grow rapidly via gravity-enhanced collisions to form planetary embryos and planets.

[25] Here we are most interested in the earlier stages of this process, wherein "hit and stick" collisions between micrometer to centimeter-sized objects is the dominant growth mechanism. The lifetime of the gas disk is up to 5 million years and so is much longer than the timescale of planetesimal accretion. We therefore adopt a simple, time-independent temperature and density radial profile for gas in a minimum mass solar nebula following [*Hayashi*, 1981]

$$T_{gas} = 280 R^{-1/2} \mathrm{K} \tag{1}$$

$$\rho_{gas} = 1.36 \times 10^{-6} R^{-11/4} \mathrm{kg\ m^{-3}} \tag{2}$$

where R denotes distance from the sun in AU (see Table 1). We first consider a time-independent, locally uniform

background magnetic field and discuss this assumption further in section 4.3.

2.3. Particle-Particle Collisions

[26] Solid particles in the nebula periodically encounter each other in non-sticking collisions. Such collisions impart high rotational velocities to the participating grains [e.g., *Wurm et al.*, 2005]. In order for magnetic alignment to overcome the effect of mutual collisions, two conditions must be met. First, the timescale of mutual particle collisions must be much longer than the timescale for a particle to come to rotational rest via gas drag. In the solar nebula, gas drag is the primary process by which particle angular momentum may be dissipated. Second, the strength of the background magnetic field must be sufficiently strong to align the particles within the timespan between successive collisions.

[27] We constrain the collision timescale t_{coll}, which can be estimated simply: $t_{coll} = (\sigma n v_{rel})^{-1}$ where σ is the interaction cross-sectional area of the particles, n is their number density, and v_{rel} is a typical relative velocity. Because most particles are relatively weakly magnetized, there should be little magnetic enhancement of their interaction cross-sectional area such that σ is $\pi(2r_p)^2$, where r_p is the particle radius. If we assume a uniform size distribution of spherical particles, we obtain

$$t_{coll} = \frac{\rho_p}{3 v_{rel} \rho_s} r_p \tag{3}$$

where ρ_p is the density of the particle and ρ_s is the volume density of solids at the specified radius in the solar nebula. We adopt a single grain density of ρ_p = 2000 kg m^{-3} as representative of a mix of compact particles such as CAIs and chondrules with highly porous dust agglomerates. The value of ρ_s for a given particle size and location depends on the assumed surface density (σ_s, in kg m^{-2}) and the scale height (H_{dust}) of the dust sub-layer:

$$\rho_s = \frac{\sigma_s}{H_{dust}}. \tag{4}$$

[28] We adopt a simple model for the surface density based on the present-day radial distribution of solid matter in the solar system [*Hayashi*, 1981]

$$\sigma_s = 300 R^{-3/2} \text{kg m}^{-2}. \tag{5}$$

[29] The scale height of the dust sub-layer depends on the assumed degree of turbulence, since a more turbulent nebula stirs the solid particles into a thicker sublayer. Its value can be estimated for a given scale height of the entire gas disk and an assumed degree of turbulence, which can be parameterized by the dimensionless quantity α. We combine a simple power law for the gas disk scale height [*Nakagawa et al.*, 1986] with the considerations on turbulence given by *Dubrulle et al.* [1995] to obtain

$$H_{dust} = 0.0472 \left(\frac{1}{3}\right)^{1/4} \sqrt{\frac{\alpha}{\Omega_k t_f}} \left(\sqrt{1 + \frac{\alpha}{\sqrt{3}\Omega_k t_f}}\right)^{-1} R^{5/4} \text{AU}. \tag{6}$$

where R is given in AU, Ω_k is the Keplerian orbital frequency, and t_f is the timescale in which a particle slows to $1/e$ of its original translational velocity due to gas drag. For particles smaller than the mean free path of gas molecules, this is given by [*Weidenschilling*, 1977]

$$t_f = \frac{\rho_p r_p}{\rho_{gas} \bar{c}} \tag{7}$$

where $\bar{c}$ is the mean velocity of gas molecules in the gas center of mass frame.

[30] We assume a uniform particle size based on results from recent numerical simulations of bouncing dust collisions [*Zsom et al.*, 2010]. When compared to a size distribution heavily skewed towards smaller agglomerate sizes such as in the dust collision simulations of *Weidenschilling* [1984], equation (3) underestimates t_{coll} for all but the largest particles (those within one order of magnitude of the maximum particle size assumed in the distribution). Finally, the characteristic particle-particle velocity (v_{rel}) for a given particle size and location depends on the state of nebular turbulence. We adopt an analytic estimate valid for small particles with $t_f < \Omega_k$ [*Cuzzi and Hogan*, 2003, equation 22].

2.4. The Rotational Gas Damping Timescale

[31] The decay of rotation due to gas damping plays two key roles. Firstly, as mentioned in the previous section, some damping is necessary to bring particles to near rotational rest. Compass needle alignment is possible only when the particle has no appreciable rotational energy retained from the most recent mutual collision. This is because if the particle is spinning sufficiently quickly, the magnetic torque will lead to precession of the rotation axis around the field direction instead of alignment (section 2.5). Secondly, the magnitude of gas drag determines the timescale of magnetic alignment (section 2.6), which must be shorter than the collisional timescale for magnetic alignment to proceed to completion. To calculate the timescale of angular deceleration of a particle, we evaluate rotational gas drag in the free molecular (FM regime, $Kn > 1/8$) and the low Reynolds number continuum (LR, $Kn < 1/8$, $Re < 1$) regimes, where the Knudsen number Kn is the ratio of the mean free path of gas molecules to the diameter of a solid particle [*Lord*, 1964]. The Reynolds number is defined as $Re = r_p^2 \rho_{gas} \omega / \eta$ where ω is the angular velocity and η is the viscosity of the gas medium. Physically, the FM flow regime corresponds to an extremely rarefied gas where the mean free path length of gas molecules is long compared to the particle size. Molecules can therefore be thought of as independent impactors onto the particle surface. By comparison, the gas particles in the continuum regime will interact with each other within the vicinity of the particle, thereby leading to boundary layer formation. The torques due to gas drag in these two regimes are given by the following expressions [*Lord*, 1964]:

$$\tau_{FM} = \frac{2\pi}{3} f \rho_{gas} \bar{c} r_p^4 \omega \tag{8}$$

$$\tau_{LR} = 8\pi\eta r_p^3 \omega \tag{9}$$

where f is the efficiency factor of momentum transfer that we assume to be 1. The equations of motion governing the decay of angular velocity over time are of the form

$$\omega' + \frac{\tau_{FM,LR}}{I}\omega = 0 \tag{10}$$

where $\tau_{FM,LR}$ denotes either τ_{FM} or τ_{LR} as appropriate for the particle, and I is the moment of inertia of the particle (approximated to be a uniform sphere). The solutions to the equations of motion are given by exponential functions:

$$\omega_{FM}(t) = \omega_0 e^{-(\tau_{FM}/I)t} \tag{11}$$

$$\omega_{LR}(t) = \omega_0 e^{-(\tau_{LR}/I)t} \tag{12}$$

where ω_0 is the initial angular velocity immediately after a particle-particle collision. The angular velocity in both regimes decreases by $1/e$ in the timescale $I/\tau_{FM,LR}$ [*Weidenschilling*, 1977]:

$$t_{FM} = \frac{4\rho_p}{5f\rho_{gas}\bar{c}} r_p \tag{13}$$

$$t_{LR} = \frac{\rho_p}{15\eta} r_p^2. \tag{14}$$

[32] In the sections below, we use the generic variable t_{drag} to denote this timescale of particle spin down, which is equal to t_{FM} or t_{LR} as appropriate for the particle and its environment. The values of t_{drag} for chondrule-sized particles are on the order of 10^2 to 10^4 seconds. This is consistent with the results of *Tsuchiyama et al.* [2003].

2.5. Precession Around the Background Field Direction

[33] In a macroscopic analog to the Larmor precession of atomic nuclei and electrons, dust grains with significant angular velocity will precess around the axis parallel to the background magnetic field. As a result, a grain that has undergone a recent particle-particle collision will precess around rather than directly align to the magnetic field. Precession is the dominant motion of the grain until its angular velocity has slowed sufficiently such that the magnetic torque can alter the particle's rotation axis in a timescale less than the rotational period of the particle. Equivalently, the rotational energy of the grain must be on the order of, or smaller than, the work done by the magnetic torque over an angle of one radian [*Davis and Greenstein*, 1951]:

$$\tau_B \gtrsim \frac{1}{2} I\omega^2 \tag{15}$$

where τ_B is the torque due to the magnetic field and ω is the remaining angular speed of the particle from the most recent disruption event. We have shown in section 2.4 that, regardless of the initial angular velocity of a particle after collision, ω decays according to an exponential function with timescale t_{FM} or t_{LR} depending on the appropriate drag law. The condition on τ_B in equation (15) becomes

$$\tau_B \gtrsim \frac{1}{2} I\omega_0^2 e^{-2t/t_{drag}} \tag{16}$$

where ω_0 is the initial angular velocity of the particle imparted in a collision and t is the time elapsed after the collision. A maximum value of ω_0 can be estimated by equating the energy of the colliding particles to the rotational energy of one of the particles immediately after the collision, which yields the approximation

$$\omega_0 \approx \frac{v_{rel}}{r_p}. \tag{17}$$

[34] We find that, under turbulent conditions ($\alpha = 10^{-2}$), ω_0 is on the order of several times 10^3 sec^{-1} for millimeter-sized particles and several times 10^2 sec^{-1} for centimeter-sized particles. Direct observations of particle rotation as observed in high speed dust collision experiments broadly agree with these estimates. One pair of photographs from *Wurm et al.* [2005] shows two 1 mm grains each rotating half a revolution in 0.5 ms ($\omega_0 \approx 6000$ sec^{-1}), although it is conceivable that one or both grains rotated an odd multiple of that number. These values are also roughly consistent with the angular velocities inferred by *Tsuchiyama et al.* [2003], who estimated chondrule angular velocities of between 300 and 2000 s^{-1} from their oblate shapes that formed during solidification.

[35] The rotational kinetic energy of a particle immediately after collision is much larger than any reasonable estimate of magnetic torque in the solar nebula (see section 2.6). Magnetic alignment is therefore not possible for the first several gas drag timescales until the rotational kinetic energy decays to the requisite levels. Whether a particle can align to the background field hinges on whether this angular velocity decay occurs quickly compared to the timescale between successive collisions.

2.6. Torque and Timescale of Magnetic Alignment

[36] The torque on a magnetic particle with mass-specific magnetic moment j in a background field with strength B_u is approximately

$$\tau_B = \frac{4\pi}{3}\rho_p r_p^3 j B_u. \tag{18}$$

[37] Laboratory measurements of the magnetic properties of natural and simulated early solar system material constrain the value of j. The value of ~220 Am^2 kg^{-1} adopted by *Nübold and Glassmeier* [2000] is certainly an upper limit because idealized single-domain crystals of pure iron were assumed. Experimental studies with metallic iron and oxides reacting under simulated conditions of the hot early solar nebula produced sub-micron sized spherules with specific moments on the order of 10 Am^2 kg^{-1} (note: 1 Am^2 kg^{-1} = 1 emu g^{-1}) [*Wang et al.*, 2010]. A more conservative estimate is given by the natural remanent magnetization (NRM) of chondrules. Laboratory measurements of chondrules and CAIs in the Allende CV carbonaceous chondrite show a

range of magnetizations from 10^{-5} to 10^{-1} Am^2 kg^{-1}. The lower end of this range is consistently lower than analogous values for fine-grained chondritic matrix, which may have been magnetized in post-accretionary processes [*Carporzen et al.*, 2011]. We adopt the value of $j = 10^{-5}$ Am^2 kg^{-1} as a reasonable, conservative estimate in our calculations. Furthermore, we conservatively adopt a value of 10 μT for the background field strength, consistent with simulations of midplane magnetic field strengths in the solar nebula [*Turner and Sano*, 2008].

[38] We can now show that the magnetic torque is small compared to the rotational energy of a particle immediately after collision and is therefore unable to cause alignment until particle rotation has decayed (equation (16)). For a 1 mm chondrule in a strong 100 μT field, the magnetic torque is 10^8 times smaller than the initial rotation energy given $\omega_0 \approx 10^3$ s^{-1} (see section 2.5).

[39] We will compare the magnitude of magnetic torque to that of other torques on the grain in the sections below. However, dominance of the magnetic torque over other effects alone is insufficient for successful grain alignment: the alignment must also occur quickly before grain orientation is disrupted by particle-particle collisions. We therefore calculate the timescale of compass needle alignment in a background field of a given strength and proceed to establish a minimum field strength necessary to bring a particle into alignment given a limiting timescale.

[40] We are only interested in particles with t_{coll} much larger than the angular velocity decay timescale (t_{FM} or t_{LR}); otherwise precession would preclude alignment. Therefore, the particles may be treated as having essentially no initial angular velocity. Defining $\theta(t)$ to be the angle between the direction of the uniform magnetic field and the dipole moment of the particle, the angular equation of motion is

$$\theta'' + I^{-1}\left[\tau_{FM,LR}\theta' + B_u J_p \sin\theta\right] = 0 \tag{19}$$

where the second term is due to rotational gas drag and the third term is the magnetic torque. Here J_p is the total dipole moment of the particle and is given by the product of j and particle mass. We can approximate this system as a damped harmonic oscillator by setting $\sin\theta \approx \theta$. In the critical and overdamped cases, the timescale of rotation from an arbitrary initial orientation to the background field is on the order of the timescale of rotational gas damping (t_{drag}). Rotation of a ferromagnetic particle to the background field cannot occur faster than this timescale; even in the presence of an arbitrarily strong magnetic field, the particle would oscillate around the field orientation, coming into alignment only after gas drag has dampened the amplitude of its oscillation. The background field strengths above which particle rotation occurs on the order of t_{drag} can be found by finding the value of B_u such that the grain is critically damped [e.g., *Taylor*, 2005]:

$$B_{FM} = \frac{5f^2\rho_g^2\bar{c}^2}{32\rho_p^2 j} \tag{20}$$

for particles in the FM regime of rotational gas drag and

$$B_{LR} = \frac{45\eta^2}{2\rho_p^2 r_p^2 j} \tag{21}$$

in the LR regime. Note that in all damping scenarios, as long as the particle belongs to the free molecular rotational drag regime, the value of B_{FM} does not depend on the size of the particle, whereas in the low Reynolds number regime, larger particles become critically damped in weaker magnetic fields. Under solar nebula conditions, critical field strengths B_{FM} and B_{LR} are very weak, below 1 μT for all locations outside of 0.5 AU. Exact numerical solutions of equation (19) corroborate these findings and validate the approximation of simple harmonic motion. Therefore, all grains under consideration in this work are in the underdamped regime, in which rotation from rest into alignment with the background field takes place in a timespan of approximately t_{drag}.

[41] We can now define t_{align}, which is the time required for alignment to the magnetic field after a mutual particle collision. This quantity is the sum of contributions from both the decay time of the angular velocity to the requisite levels (section 2.5) and the time of rotation to the magnetic field. The former contribution (t_{prec}) can be found by combining equations (16) and (18):

$$t_{prec} = -\frac{1}{2}\ln\frac{5B_u j}{r_p^2\omega_0^2}t_{drag}. \tag{22}$$

[42] Because the subsequent rotation of the magnetic particle to the background field takes place in the timescale t_{drag} in the underdamped regime, the total time of alignment is

$$t_{align} = \left(1 - \frac{1}{2}\ln\frac{5B_u j}{r_p^2\omega_0^2}\right)t_{drag}. \tag{23}$$

[43] Under solar nebula conditions, the precession term in equation (23) (second term) is typically one order of magnitude greater than the magnetic rotation term.

2.7. Brownian Motion

[44] The orientations of very small magnetic grains are subject to the randomizing effects of rotational Brownian motion. Grains behave in this regime when the rotational component of thermal energy ($kT/2$) is comparable to the magnetic energy of alignment. Assuming thermal equilibrium, the grain size at which this occurs (r_{Br}) can be estimated conservatively as [*Collinson*, 1965; *Tauxe et al.*, 2006]

$$\frac{4\pi}{3}\theta_{crit}^2\rho_p B_u j r_{Br}^3 \approx kT_{gas} \tag{24}$$

where k is the Boltzmann constant, B is the strength of the background field, and θ_{crit} is the allowed angular deviation from perfect alignment. We adopt a value of $\theta_{crit} = \pi/10$ as our threshold for an "aligned" particle. This simple analysis neglects the inertia of the grain and viscous drag forces, which decrease the effect of random thermal rotations. Therefore, our estimate for r_{Br} should be regarded as an upper bound, and some particles smaller than this threshold may not be strongly affected by rotational Brownian motion.

2.8. Aerodynamic Torque

[45] Non-spherical particles with Reynolds number greater than about 0.1 tend to align their long axis perpendicular to

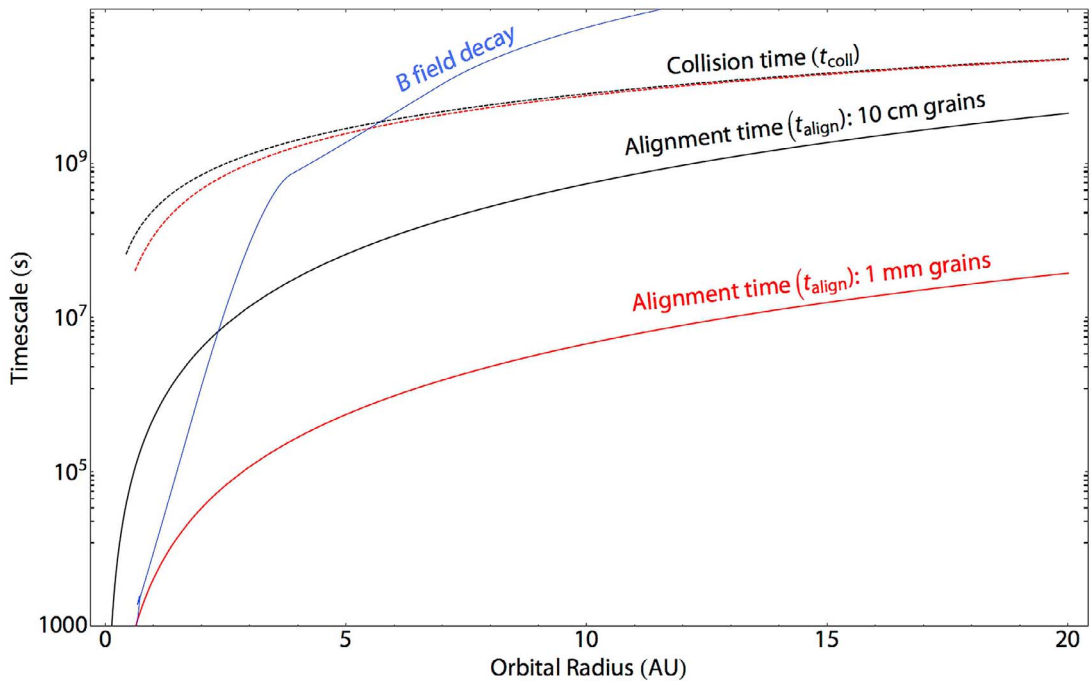

Figure 1. The expected timescales of successive particle to particle collisions (dotted curves, t_{coll}) compared to timescales of alignment to the local magnetic field of strength 10^{-5} T (solid curves, t_{align}). The alignment timescale includes contributions from both the spin down in angular velocity and the rotation of a particle at rest to the magnetic field direction. The spin down contribution is 8–11 times that of magnetic rotation for particles between 100 μm and 10 cm in size in the solar nebula. The blue curve indicates the expected timescales of magnetic field diffusion in a late-stage solar nebula with large accreted particles 1 cm in size [*Stepinski*, 1992]. ADRM may be active where these diffusion timescales are longer than those of magnetic alignment.

their direction of motion within laboratory timescales of a few seconds [e.g., *McNown and Malaika*, 1950]. This mechanism has been proposed as a key factor limiting the maximum particle size that is able to participate in terrestrial DRM [*Heslop*, 2007]. Particles in water on Earth tend to align to their hydrodynamically preferred orientation when they are larger than about 10 μm for ellipsoidal particles with aspect ratios (ratio of major to minor axes) of $\chi = 1.1$. As the timescale available for alignment is long in the solar nebula (Figure 1), particles with Reynolds numbers smaller than 0.1 may also align to the wind direction unless the magnetic torque is greater in magnitude. We therefore evaluate the magnitude of the aerodynamic torque in both FM and LR regimes. In both cases, for the sake of simplicity, we consider prolate ellipsoidal particles of homogenous density where r_p now refers to the minor axis radius and χ equals 1.1 and 2 to simulate a range of non-sphericities.

[46] In the FM regime, the overall torque is found by a sum of contributions from individual gas molecule collisions on all parts of the body. We use the expression for torque from each surface element as derived by *Ivanov and Yanshin* [1980, equation 3], who assumed a Maxwellian velocity distribution of gas molecules and thermal equilibrium with the solid particle.

[47] For torque due to Stokes flow in the LR regime, we follow *Galdi and Vaidya* [2001] and *Heslop* [2007]. The aerodynamic torque τ_a on a symmetrical prolate ellipsoid with semi-minor axis radius r_p and eccentricity $e = \sqrt{1-\chi^{-2}}$ is

$$\tau_{asym,LR} \approx \frac{16\chi^4 r_p^4 \rho_{gas}^2 v_{gas}^3 |G|}{\eta} \sin(2\phi)\sqrt{\frac{\sin^2\phi}{Y^2}+\frac{\cos^2\phi}{X^2}} \cdot \left\{\cos(2\phi)\left[\left(\frac{\cos\phi}{X}\right)^2-\left(\frac{\sin\phi}{Y}\right)^2\right]-\frac{\cos(4\phi)}{2XY}\right\} \quad (25)$$

where

$$X = \frac{8}{3}e^3\left[-2e+\left(1+e^2\right)\ln\left(\frac{1+e}{1-e}\right)\right]^{-1}$$

$$Y = \frac{16}{3}e^3\left[2e+\left(3e^2-1\right)\ln\left(\frac{1+e}{1-e}\right)\right]^{-1}.$$

[48] The torque coefficient $|G|$ varies between 0 and 1 and is a function of e, ϕ is the angle between the long axis of the particle and the plane perpendicular to the flow axis, and v_{gas} is the relative velocity between the particle and surrounding gas. The angle ϕ is estimated as $\pi/4$ to yield a value of torque close to the maximum. The velocity v_{gas} is estimated with a combination of systemic drift (due to different orbital velocities of solids and gas) and turbulence contributions.

The former contribution is calculated explicitly by simultaneously solving equations 15 and 20 in the work of *Weidenschilling* [1977]. The latter velocity component due to turbulence is estimated for two scenarios. First, we assume a quiescent nebula with zero turbulent velocity [*Zsom et al.*, 2010] in order to find a lower bound on the aerodynamic torque. Second, we assume a highly turbulent nebula ($\alpha = 10^{-2}$; [*Dubrulle et al.*, 1995]). To simulate the instances of maximum particle-gas velocity we add the drift and turbulent contributions of velocity (as opposed to adding in quadrature). Following the notation of *Cuzzi and Hogan* [2003], the turbulent component of particle-gas velocity, v_{turb}, is

$$v_{turb} = v_g \left[\frac{St_L^2 \left(Re^{1/2} - 1 \right)}{(St_L + 1)(St_L Re^{1/2} + 1)} \right]^{1/2} \tag{26}$$

where v_g is the root mean square local velocity of gas relative to its own center of mass frame given by $v_g = \bar{c}\alpha^{1/2}$. The Stokes number St_L is defined as the ratio of the translational gas stopping timescale (t_f) to the overturn timescale of the largest eddy, which is on the order of the local orbital period. The flow Reynolds number Re is defined as

$$Re \equiv \frac{L v_g \rho_{gas}}{\eta} \tag{27}$$

where L is the size scale of the largest eddy, which is equal to the local scale height of the gas in the accretion disk [*Nakagawa et al.*, 1986]. Values used in this work for α are between 10^{-4} and 10^{-2}, which are consistent with nebular turbulence generated by the MRI [*Balbus and Hawley*, 2000]. Employing the derived velocities, we calculate the aerodynamic torque and compare it to the torque of the background magnetic field, τ_B.

[49] In addition, we note *Gold* [1952] proposed that supersonic flow of a dilute gas across an ensemble of elongated particles would produce dust grain angular momentum vectors in the plane perpendicular to the direction of gas flow. The reasoning is that each impact between a grain and a molecule in an unidirectional stream contributes a small angular momentum that is described by a vector confined to the perpendicular plane. Given a large number of such collisions, a significant net angular momentum vector will result. This effect is only valid for fast, rarified, and unidirectional gas flows such that the angular momentum contribution from each gas molecule collision is independent of the orientation and angular velocity of the grain. Specifically, the gas flow velocity across the grain must be supersonic so that only the faces of the grain oriented towards the flow direction receive momentum from the gas [*Lazarian*, 2007]. However, the gas environment within the solar nebula is sufficiently dense and warm such that grain motion is dominated by gas molecule collisions on all faces of the grain both towards and away from the wind direction. The mean gas particle velocity at 20 AU, for example, is $\bar{c} = 745$ m s^{-1}, while particle drift velocities relative to the wind are no higher than several times 10 m s^{-1}. The Gold mechanism therefore cannot be a significant source of angular momentum for dust grains in the inner solar nebula.

2.9. Accommodation Torque

[50] Random heterogeneities in the momentum transfer coefficient (f, or the accommodation coefficient) on the surface of grains can result in a small net torque due to the bombardment of many gas molecules. *Purcell* [1979] first studied this effect and showed that the rotational energy from this source compared to the thermal excitation is

$$\frac{E_{accom}}{kT_{gas}} \approx 7 \times 10^6 \left(\frac{S\delta}{r_p} \right)^2 \tag{28}$$

where S is the characteristic size scale of surface heterogeneities and δ represents the magnitude of contrast in the accommodation coefficient. The latter quantity is estimated to range between 0.01 and 0.1, while S can be estimated by the mineral grain size observed in primitive materials. We therefore follow *Purcell* [1979] and adopt 10^{-7} m as our estimate for S. We use $\delta = 0.1$ to simulate a high degree of variability in the accommodation coefficient.

2.10. Radiative Torque

[51] Incident radiation can result in a torque on irregularly shaped grains. This effect was first proposed by *Dolginov and Mytrophanov* [1976], who considered the case of polarized incident radiation. The full magnitude of radative torque due to a general radiation field was not appreciated until the numerical simulations of *Draine and Weingartner* [1996], who showed that this effect may be the primary source of grain angular momentum in the ISM for particles of size greater than $\sim$0.1 μm. Torque on a grain in a radiation field with volume energy density u_{rad} and mean wavelength $\bar{\lambda}$ can be estimated by

$$\tau_{rad} \approx \frac{1}{2} r_p^2 u_{rad} \bar{\lambda} Q_\Gamma \tag{29}$$

where Q_Γ is the radiative "torque efficiency," which is specific for each grain shape and orientation with respect to any anisotropic radiation field. The value of Q_Γ generally varies by within a factor of a few for a variety of distinctly shaped irregular particles [*Lazarian and Hoang*, 2007]. A representative value of Q_Γ can be estimated as a function of the size of the particle and the characteristic wavelength of the impinging radiation. For particles larger than the typical wavelength ($r_p/\bar{\lambda} \geq 1$), Q_Γ is on the order of unity, while $Q_\Gamma \approx \left(r_p/\bar{\lambda} \right)^3$ for $r_p/\bar{\lambda} < 1$ [*Cho and Lazarian*, 2007]. We adopt this approximation for our analysis. In reality, Q_Γ is suspected to decrease for particles much larger than the wavelength of radiation ($r_p/\bar{\lambda} \lesssim 10$) due to the mutually incoherent torque contributions from a large number of grain facets. Numerical simulations for such large grains have not yet been carried out due to the computational costs involved. Radiation in the dust-sublayer of the solar nebula is dominated by in situ blackbody radiation in the far infrared, peaking at $\sim$100 μm. Therefore, our values for τ_{rad} represent an upper bound for grains larger than about 1 mm.

[52] Radiation with wavelengths shorter than the above peak value is expected to be reradiated from dust that is exposed to sunlight at the top and bottom surfaces of the disk. However, this reradiated light is greatly attenuated in the

deep interior of the disk within the dust sub-layer [*Chiang and Goldreich*, 1997]. The radiation energy density is therefore a function of the interior temperature of the disk (equation (1)). The energy density inside a blackbody emission region at temperature T integrated over all wavelengths is given by Planck's Law:

$$u_{rad} = \frac{8\pi^5 k^4}{15c^3h^3} T^4 \tag{30}$$

where k is Boltzmann's constant, h is Planck's constant, and c is the speed of light.

2.11. Purcell Torque

[53] Purcell torque arises from heterogeneities on grain surfaces that result in variations in the rate of H_2 formation. Molecular hydrogen (H_2) formation in the ISM occurs primarily when individual H atoms are adsorbed onto the surface of dust grains where they encounter each other and depart as newly formed H_2. This recombination process occurs preferentially at "enhanced sites" where the binding energy between the grain and H atom is anomalously high. At such locations, H atoms are prevented from leaving the grain surface for a timespan longer than from other locations, thereby increasing the probability of an H_2 formation reaction [*Hollenbach and Salpeter*, 1971]. Because these sites are not uniformly distributed across the surface of the grain, unbalanced reaction forces from the departure of H_2 molecules result in a net torque on the grain. *Purcell* [1979] estimated this torque to be

$$\tau_{Purcell} \approx \sqrt{\frac{32}{3\pi}} \gamma r_p^3 n_H \sqrt{\frac{kTE_{H_2}}{\nu}} \tag{31}$$

where γ is the fraction of H atoms that leave the grain as H_2 molecules, n_H is the number density of atomic hydrogen, E_{H_2} is the kinetic energy of an ejected H_2 molecule, and ν is the number of "enhanced sites" on the grain. For the elevated temperatures in the solar nebula, γ is approximately 0.2 [*Cazaux et al.*, 2005]. The relative abundance of atomic to molecular hydrogen (n_H/n_{H_2}) in protoplanetary disks is less than 10^{-4} at 1 AU [*Glassgold et al.*, 2009]. *Willacy et al.* [1998] showed that this ratio decreases with increasing orbital radius, although they did not present the values that support this. We use the approximation $n_H/n_{H_2} = 10^{-4}$ for all radii. *Purcell* [1979] estimated E_{H_2} to be 3×10^{-20} J and ν to be on the order of 100 for a grain with radius 10^{-7} m. We adopt Purcell's figure for E_{H_2} and estimate ν for all grain sizes by scaling with the grain surface area: $\nu(r_p) = 100(r_p/10^{-7})^2$.

3. Results

[54] The analysis in the preceding section allows us to evaluate the likelihood of magnetic alignment for particles of different sizes and at distinct locations in the solar nebula. The following conditions are necessary for alignment between the grain magnetic moment and the background field:

[55] 1. Sufficient gas damping to bring a particle to near rotational rest in between successive collisions.

[56] 2. Sufficient background field strength to bring a particle to alignment between successive collisions.

[57] 3. Sufficient temporal stability of the background magnetic field direction.

[58] 4. Negligible effect of Brownian motion.

[59] 5. Small aerodynamic torque due to non-spherical particle shape compared to magnetic torque.

[60] 6. Small torques due to variations in accommodation coefficient on grain surface.

[61] 7. Small radiative torque compared to magnetic torque.

[62] 8. Small Purcell torque compared to magnetic torque.

[63] Note that these conditions can be divided into dynamical (1, 2, and 3) and equilibrium (4, 5, 6, 7, and 8) requirements. The former requirements ensure that alignment occurs quickly between disruptive events (either mutual collisions or changes in the background field) while the latter establish magnetism as the dominant source of torque on the grain. Both sets of requirements must be met in order for a ferromagnetic grain to align successfully to the background field. We refer to the grains that satisfy the dynamical requirements as "stationary" and ones that satisfy both dynamical and equilibrium requirements as "aligned."

3.1. Dynamical Requirements

[64] Grains satisfying the dynamical requirements of magnetic alignment orient to the background field quickly before another event disrupts their alignment. As discussed in section 2.5, gas drag must slow the angular velocity of grains sufficiently such that their rotational energy is on the order of the magnetic work over one radian of rotation. This spin down occurs over the timescale t_{prec}. In addition to the time required for grain spin down due to gas drag, an additional timespan is required for the magnetic field to rotate the grain from an arbitrary orientation into alignment. For fields stronger than the critical strength indicated in equations (20) and (21), this rotation timescale is on the order of t_{drag}. Under solar nebula conditions, this critical field strength is very weak, below 1 μT for all locations outside of 0.5 AU. Therefore, the total time elapsed between a particle-particle collision and magnetic alignment (t_{align}) is the sum of these two contributions ($t_{prec} + t_{drag}$) and is given in equation (23).

[65] At the same time, the expected time between particle-particle collisions (t_{coll}) for a given r_p and R can be estimated by combining equations (3) through (7) in section 2.3. Particles of a given size and at a given radius in the disk spend some fraction of time at rotational rest (i.e., they are stationary particles) if $t_{coll} > t_{align}$. Mutual collisions between solid particles do not prevent magnetic alignment for such particles. In the inner 10 AU of the disk, most grains smaller than 1 m in diameter in a 10^{-5} T field are stationary (Figure 2).

[66] A maximum in the possible size range of stationary particles occurs at about 4 AU (Figure 3, black curve). The existence of this maximum can be explained as follows. At this orbital radius, the gas drag law governing the largest stopped particle transitions from the LR regime at smaller orbital radii to the FM regime. The stopping time of particles of a given size in the LR regime is relatively insensitive to orbital radius ($t_{LR} \propto R^{1/4}$). On the other hand, at all orbital radii, t_{coll} increases quickly for particles farther from the sun ($t_{coll} \propto R^{3/2}$). Therefore, as one moves innerward from 4 AU, t_{coll} decreases faster than t_{align}, making stopping more difficult. As such, only smaller particles, which always have

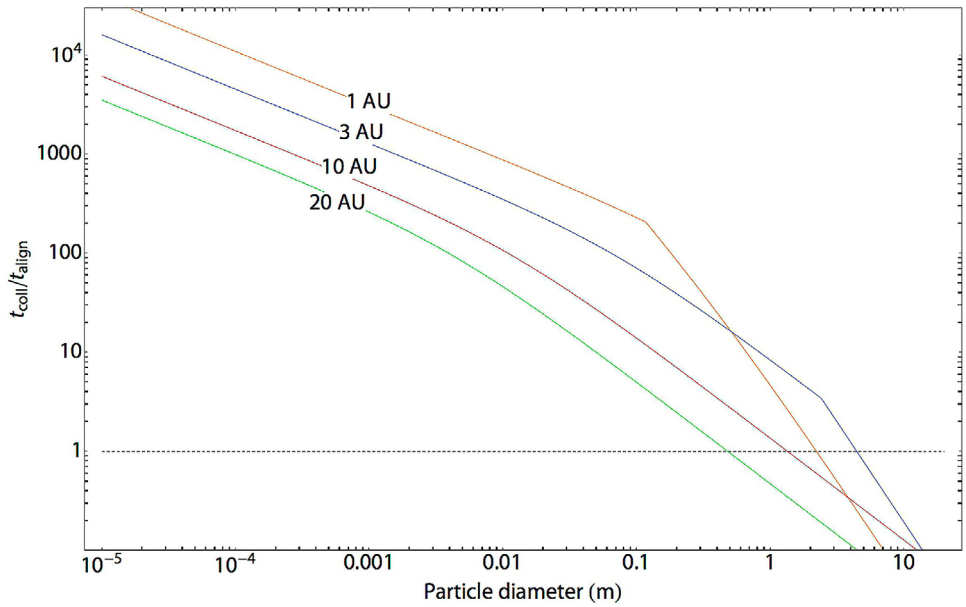

Figure 2. The ratio of average time between mutual collisions (t_{coll}) and minimum time necessary for particles to spin down and align to the background field following a mutual collision (t_{align}) for a range of particle sizes and locations in the solar nebula. Assumed background field is 10^{-5} T. Particles with the ratio $t_{coll}/t_{align} \gg 1$ have negligible angular velocity at most times and would align to the magnetic field if no stronger torque acts on them. The discontinuity in the curves at 1 and 3 AU is due to transition of the rotational drag law from the FM to LR regime.

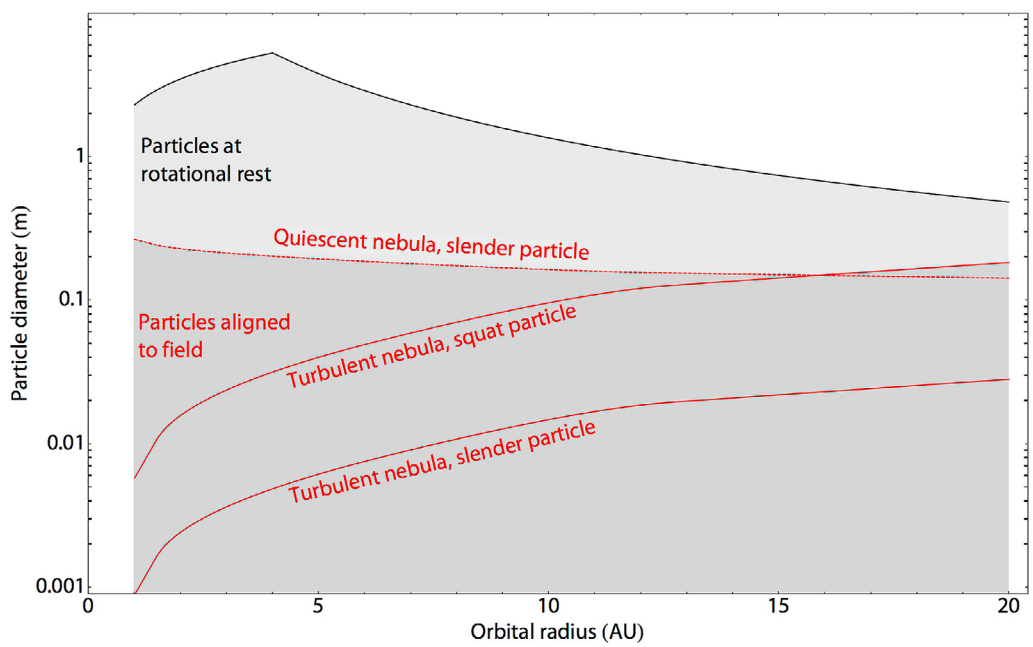

Figure 3. Expected maximum particle sizes to reach magnetic alignment. The solid black curve shows the maximum size of a particle that can be efficiently brought to rotational rest within the timescale of successive collisions ($t_{coll} = t_{align}$) for a background field strength of 10^{-5} T. The set of three red curves show the maximum semi-minor axis diameter of an elongated particle ($\chi = 2$ for "thin" and $\chi = 1.1$ for "squat" particles) for which magnetic torque is greater than aerodynamic torque. The "Quiescent Nebula" case assumes relative velocity due to only radial drift while the "Turbulent Nebula" case assumes $\alpha = 10^{-2}$. Dark grey zone delineates particle sizes that reach alignment with the field between successive collisions, light grey zone delineates particles that come to rotational rest between collisions but do not align with the background field between successive collisions, and white zone delineates particles that remain continuously in motion between successive collisions.

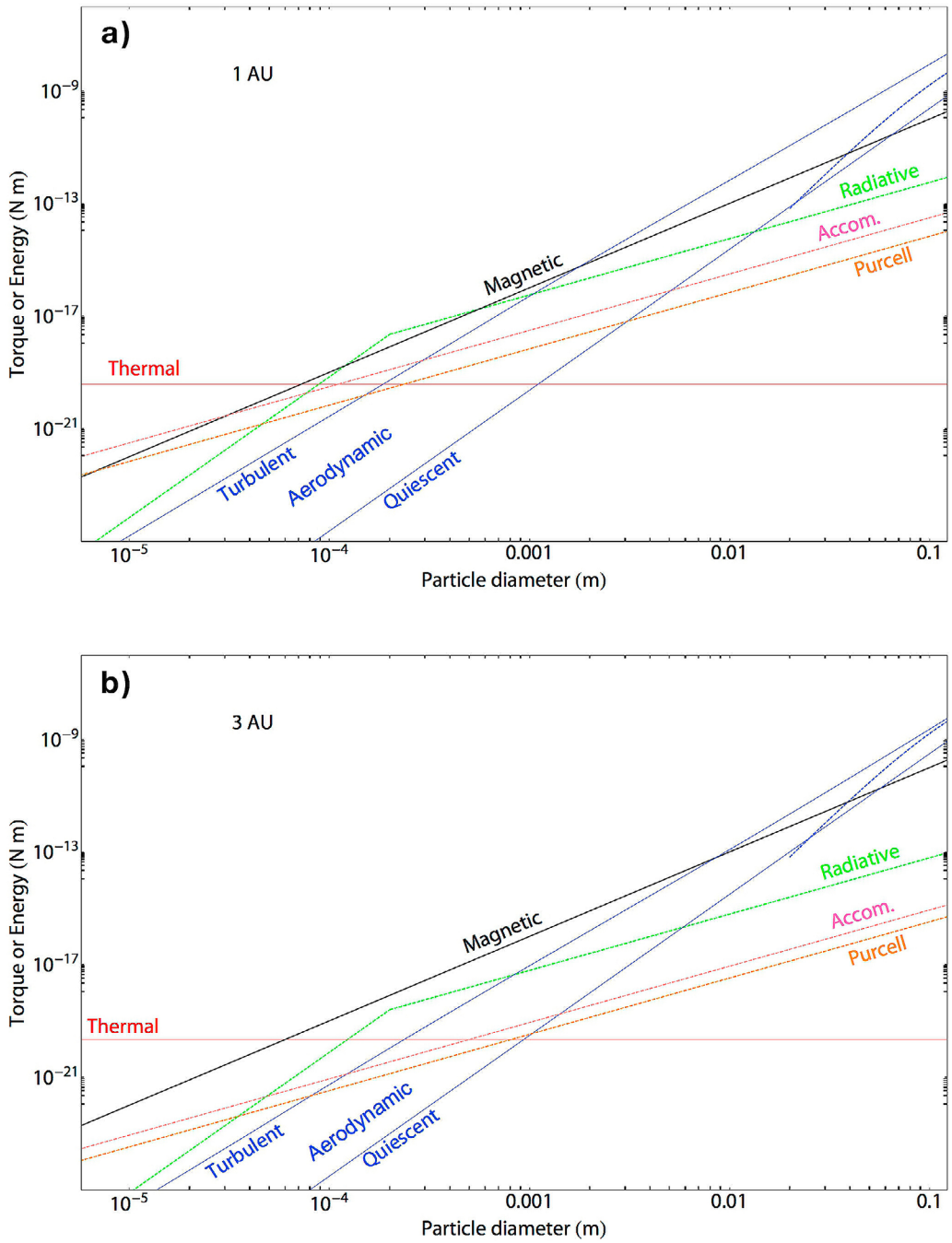

Figure 4. A comparison of the magnitudes of static and thermal excitation as a function of particle size for a background field of 10^{-5} T. The upper and lower solid blue lines were calculated for prolate ellipsoids in the FM regime with 1:2 and 1:1.1 aspect ratios, respectively. The dashed blue line represents torque in a turbulent nebula on a 1:2 ellipsoid in the LR regime, which applies for particle sizes of $\gtrsim$7 cm. Particles in the size range where the magnetic torque is dominant are expected to come to alignment with a uniform magnetic field. "Accom." is short for accommodation torque (section 2.9).

shorter values of t_{align} at the same orbital radius than larger particles, are able to stop, resulting in the decreasing range of stopped particle sizes at $R < 4$ AU. On the other hand, due to the more rarified gas environment, the largest stopped particles at $R > 4$ AU are in the FM regime, where t_{align} is very sensitive to orbital radius ($t_{align} \propto R^3$). As one moves away from the sun beyond 4 AU, t_{align} increases more rapidly than t_{coll}, resulting in more difficult stopping and therefore a smaller range of stationary particle sizes.

3.2. Equilibrium Requirements

[67] Grains satisfying the dynamical requirements in the previous section have sufficient time between successive disruptive events to come to alignment in response to the

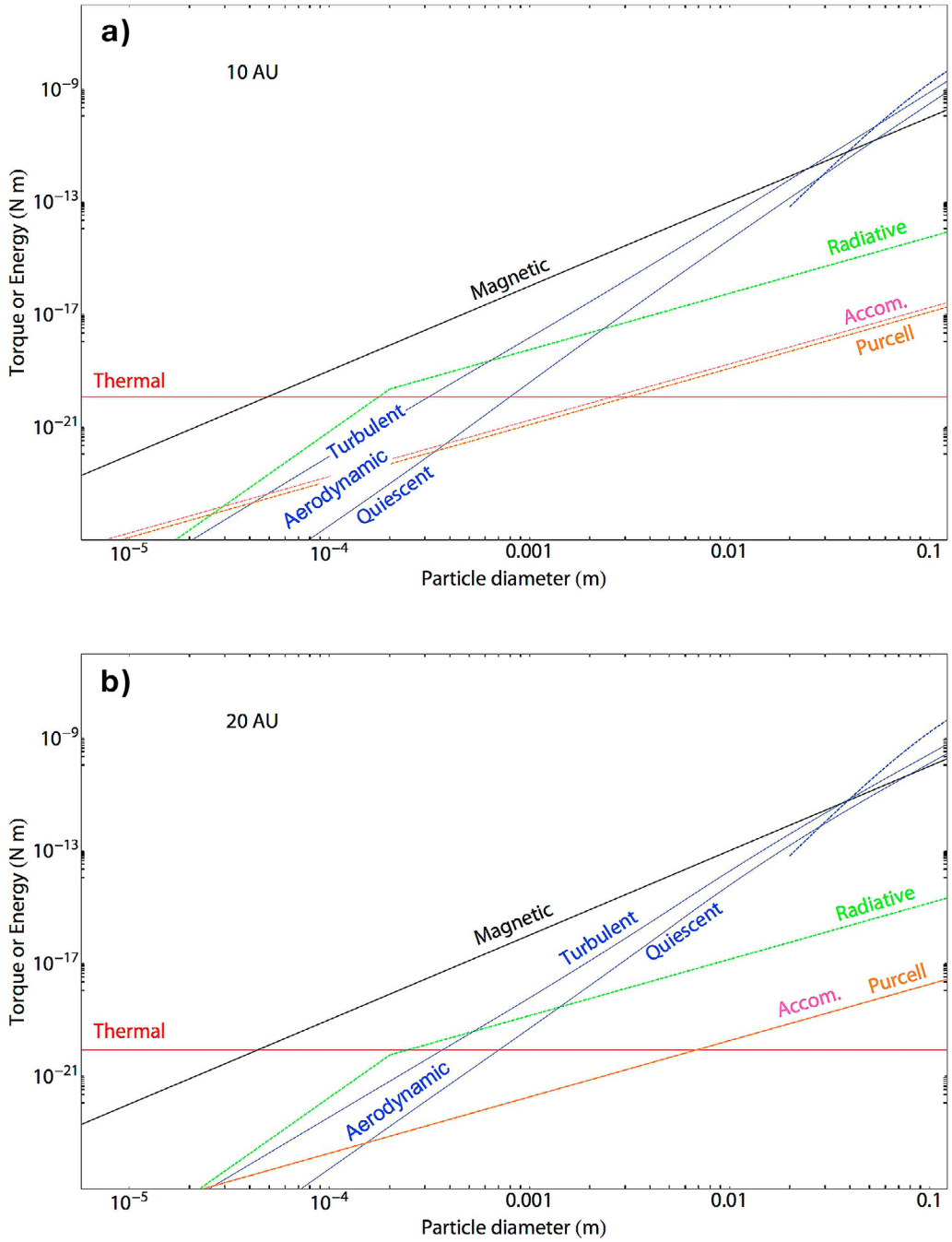

Figure 5. As Figure 4, for greater orbital radii.

strongest torque acting on the particle. Of the six candidate phenomena evaluated here (magnetic, thermal, aerodynamic, accommodation, radiative, and Purcell), we find that magnetic torque controls the orientation of spherical ferromagnetic grains within a range of sizes spanning several orders of magnitude (30 μm to several cm; Figures 4 and 5). Between $\sim$1.5 and 20 AU in the dust sub-layer of the disk, aerodynamic torques dominate for larger, non-spherical grains while thermal excitation (i.e., rotational Brownian motion) prevents the alignment of very small grains. Radiative torque is stronger than magnetic torque for small grains ($\lesssim$500 μm) in the innermost nebula ($\lesssim$1.5 AU).

[68] Non-spherical particles experience an aerodynamic torque based on their shape and direction of motion. For most locations in the solar nebula ($\gtrsim$0.2 AU), this effect imposes the upper limit on the size range of magnetically aligned particles (Figures 4 and 5). This size threshold is provided by equating the aerodynamic and magnetic torques for a range of locations in the solar nebula and for an assumed field strength. We constrain the effect of turbulence by evaluating the aerodynamic torque for a quiescent (α = 0) and highly turbulent ($\alpha = 10^{-2}$) nebula. The lower size limit for magnetic alignment is defined by Brownian motion, except for

the innermost nebula (<1.5 AU), where radiative torques dominate the alignment of grains on the order of 100 μm in size or smaller. Grains in this size range are most susceptible to radiative torque since they are close to the characteristic wavelength of the radiation field.

[69] Due to the low abundance of atomic H and the large grain sizes in the solar nebula, Purcell torque is weaker than its magnetic counterpart for grains larger than the micrometer scale. For such small grain sizes, rotational Brownian motion inhibits successful magnetic alignment in any case. With respect to torque due to heterogeneities in the accommodation coefficient (section 2.8), we find that this contribution to rotational kinetic energy is on the order of or less than 0.1 times the magnetic torque at the transition around 50 μm above which magnetic torques overwhelm thermal excitation. Magnetic torque increase quickly with respect to accommodation torque for larger grains. Therefore, this effect is not the dominant effect for grains of any diameter. Note that accommodation torque is greater in magnitude than Purcell torque (Figures 4 and 5), which is opposite of the situation in the ISM, where Purcell torque are dominant. This is due to the much lower ratio of atomic H to molecular H_2 in the solar nebula.

[70] Taken together, our models show that, in a stable, uniform 10 μT field in a turbulent nebula, non-spherical magnetic particles with sizes from several tens of μm to several cm and aspect ratios between 1.1:1 and 2:1 are expected to be aligned with the background field (Figure 3). Even larger particles greater than a meter in size may be aligned for nearly-spherical particles, although the production of extremely spherical particles may be unlikely. Particles larger than these sizes are oriented primarily due to aerodynamic torque such that further mutual accretions will no longer efficiently preserve a net dipole moment. This size range includes significantly larger particles than those aligned in terrestrial DRM, which is thought to align grains up to just several tens of μm in size [*Tauxe et al.*, 2006]. This difference is due to a combination of a much more rarefied environment (hence less gas drag and aerodynamic torque) and longer timescales of accretion compared to settling in a water column (hence allowance for longer timescales of magnetic alignment). Our predictions for ADRM also contrast with the predicted alignment of small (0.01–100 μm) grains in T Tauri disks due to radiative torque [*Cho and Lazarian*, 2007]. However, *Cho and Lazarian* [2007] did not address the effect of magnetic fields on ferromagnetic grains, for which magnetic torques dominate over radiative torques under most circumstances (Figures 4 and 5).

[71] We note that some fraction of grains may be oriented such that radiative torques induce sustained suprathermal rotation, (i.e., their rotational energy is much greater than kT) [*Lazarian and Hoang*, 2008]. In such a case, the radiative torque, although weaker than the magnetic torque in magnitude, can sustain fast rotations in dust grains, which do not undergo compass needle alignment if their rotational energy is greater than the magnitude of magnetic torque (see section 2.5). However, such suprathermal rotation is not likely to be a significant source of grain misalignment limiting ADRM for two reasons. Firstly, using the formalism given by *Lazarian and Hoang* [2008], the suprathermal rotation state is not always stable even for ferromagnetic particles. This is mainly due to the high density of gas in the solar nebula (compared to the ISM), which makes for very short gas damping timescales. Ferromagnetic particles (with a typical susceptibility enhancement of 10^3 over paramagnetic grains) larger than $\sim$ 40 μm at 3 AU (2 μm for 1 AU, 1 mm for 10 AU, 1 cm for 20 AU) have $t_{DG} > t_{drag}$. Most such particles, like paramagnetic particles, have a single stable rotational configuration with subthermal velocity [*Lazarian and Hoang*, 2007].

[72] Secondly, even if there is a stable high rotational velocity configuration for the grains, only some small fraction of grains are in the high rotational velocity state at any given time [*Lazarian and Hoang*, 2008, Figure 2b]. Therefore, although this effect may be responsible for preventing some grains from undergoing magnetic compass needle alignment, some population of grains will still be rotating slowly and therefore subject to magnetic torque. Unfortunately, we do not have access to the numerical simulations of *Lazarian and Hoang* [2008] to quantify the exact proportion of fast grains, and doing such a simulation is beyond the scope of this paper. We therefore regard suprathermal rotation as a possible means of decreasing the efficiency of alignment for a limited range of particle sizes, but cannot prevent the alignment of such grains altogether.

4. Discussion

4.1. Origin of Ferromagnetic Grains

[73] With the size range of magnetic alignment constrained (Figures 3, 4, and 5), we now discuss the likelihood of forming ferromagnetic particles within this size. In order for ADRM to operate, particles smaller than about 30 μm must grow into the size range in which ADRM is active while preserving an appreciable net magnetic moment. Specifically, the per unit mass magnetic moment must be greater than or equal to 10^{-5} Am^2 kg^{-1} to be consistent with our assumption from section 2.6. This may be achieved in three ways. Firstly, magnetic aggregates up to $\sim$1 mm may be formed due to AARM if some of the magnetic grains in the agglomerate are made of strongly ferromagnetic minerals like kamacite or magnetite [*Nübold and Glassmeier*, 2000; *Wang et al.*, 2010]. Secondly, millimeter-scale igneous particles such as chondrules and CAIs, which may have formed in great abundance in the early hot nebula [*Bockelée-Morvan et al.*, 2002], would carry a significant magnetization if they formed in the presence of a magnetic field. Thirdly, even fully random assemblages of micrometer-scale grains can maintain a significant dipole moment into the size range where alignment to a background field is expected. Monte Carlo simulations of such flocs of magnetic grains show that the specific magnetization of a 10 μm aggregate is decreased by a factor of 40 compared to that of its constituent 1 μm grains [*Heslop*, 2007]. Therefore, if individual grains are magnetized to the mid- to upper- range of values as observed in the chondrules and CAIs of the Allende CV carbonaceous chondrite ($j = 10^{-4} - 10^{-3}$ Am^2 kg^{-1} or 10^{-6} to 10^{-5} times the saturation magnetization of iron), our conservative estimate of $j = 10^{-5}$ Am^2 kg^{-1} is reasonable.

4.2. Accretion and Subsequent Processing

[74] In the preceding sections, we defined the size range of particles that are expected to align to a stable background magnetic field in the solar nebula. We now discuss the

subsequent growth of such particles into planetesimals and the necessary conditions for the preservation of ADRM on planetary bodies.

[75] Solid particles in the solar nebula took the form of compact particles (CAIs, chondrules, lithic fragments), porous dust aggregates, or a mixture of the two. Melting or condensation produced directly compact particles up to 1 cm in size (more typically ≤1 mm). Although the agglomeration of dust and compact particles is a poorly understood process, most models and experiments suggest that growth into the millimeter or even centimeter scale is possible solely due to mutual, sticking collisions [e.g., *Güttler et al.*, 2010; *Ormel et al.*, 2008; E. Beitz et al., Free collisions in a microgravity many-particle experiment. II. The collision dynamics of dust-coated chondrules, submitted manuscript, 2011]. Particles in these size ranges should be subject to magnetic alignment in the appropriate regions of the nebula (Figure 6a).

[76] Several hypotheses exist regarding the subsequent evolution of such millimeter or centimeter-sized particles. The first class of models involve the incremental growth of particles via mutual collisions. Some fraction of these collisions result in the creation of larger solid aggregates. This process continues throughout the nebula until dust aggregates reach the km size scale, whereupon gravitational attraction becomes the driving force between further agglomeration. The second class of models call on some form of instability that enhance the density of a solid particles in a localized region of the nebula. Small particles within these high-density zones then accrete to form planetesimals directly. The nature of the instability may be solely due to the mutual gravity of a large number of small particles [*Cuzzi et al.*, 2008] (Figure 6b, top) or may invoke local flow fields (i.e., streaming instabilities) of the nebular gas initially to concentrate particles [*Johansen et al.*, 2007] (Figure 6b, bottom). In the former scenario, solid particles of millimeter size are able to form gravitational instabilities directly while in the latter scenario "boulders" at least several decimeters in size are required to participate in the streaming instabilities. A third possible fate of free particles in the solar nebula is late accretion directly onto the surface of an already-formed planetesimal (Figure 6b, middle).

[77] ADRM operates differently on particles that accrete via these distinct pathways. In the incremental growth scenario, agglomeration of particles within the size range in which ADRM is active should form structures with larger and larger net magnetic moment. This process should continue until the dust aggregates have grown larger than the maximum size for effective ADRM, which may be from several millimeters to several centimeters in size (section 3.2), depending on the sphericity of the aggregate. Further agglomeration of larger dust aggregates, which are oriented to the direction of gas flow, no longer preserve a net magnetic moment. Ultimately, the accreted planetesimal would be composed of zones of uniform magnetization with a range of sizes up to the upper size limit of active ADRM. Adjacent ADRM zones may show some coherence in direction if the rate of accretion was rapid compared to the timescale of local magnetic field change (e.g., due to rotation of the parent body).

[78] In the gravitational collapse scenario, the participating particles may be in the appropriate size regime for magnetic alignment (Figure 6b, top). In such a case, the resulting planetesimal may contain large ADRM zones. Portions of the planetesimal that accreted in a stable magnetic field may show coherent magnetic moment directions. Although the high density of solids in the gravitational instability tends to make magnetic alignment more difficult, relative velocities in such concentrated clumps may be much slower than those typical in the solar nebula, resulting in more efficient magnetic grain alignment [*Cuzzi et al.*, 2008]. On the other hand, the streaming instability requires solid boulders too large for magnetic alignment. In this scenario, the boulders, and therefore the planetesimals they form, may contain ADRM zones near the upper size limit of magnetic alignment (Figure 6b, bottom). The ADRM zones in these boulders would therefore remain at the cm-size. Finally, in the case of late accretion directly onto formed planetesimals, we may expect to see zones of coherent magnetization whose size depends on the rate of accretion compared to that of planetesimal rotation or local magnetic field change (Figure 6b, middle).

[79] Can the orientation of solid particles be preserved during accretional collision? In the case of porous aggregates, some coherent grain orientations are likely preserved upon accretion. Dust collision experiments at high relative velocities of several tens of meters per second [*Wurm et al.*, 2005; *Paraskov et al.*, 2007; *Teiser and Wurm*, 2009] have shown that sticking collisions between a small porous (80–90% porosity) "projectile" and a "target" of lower porosity (but still as high as 66%) preserve a nearly intact core of the porous body accounting for between 30% and 70% of the original projectile mass. Collisions of dust aggregates may therefore result in zones of unidirectional magnetization bordered by zones of randomized grain orientations and low net magnetic moment (Figure 6c, top). The zones of unidirectional magnetization represent the intact cores of the impactor, while the interstitial regions of low magnetization represent particles whose orientations were scrambled upon impact. Disruption of particle orientations in the larger participating aggregate ("target") is more severe when it is also highly porous (80–90% porosity). On the other hand, compacted aggregates (< 66% porosity) are much more resistant to such catastrophic excavation [*Paraskov et al.*, 2007; *Teiser and Wurm*, 2009]. In the case of chondrules and CAIs, sticking collisions may or may not result in the rolling of one object across the surface of another [*Ormel et al.*, 2008]. In the former case, magnetic coherence is preserved.

[80] Subsequent impacts of compact and porous particles onto the planetesimal body likely led to significant compaction [*Weidenschilling and Cuzzi*, 2006]. Compaction of an accreted magnetic aggregate will affect the preservation of its ADRM. Studies of terrestrial DRM formation [*Anson and Kodama*, 1987] have found that compaction alone should not erase ADRM, although its magnitude can be modestly reduced (e.g., 20% reduction after 50% volume change). A later study using a wider variety of minerals showed that magnetization reduction ranged from 0.2% to 48.5%, with most samples in the 30% to 40% range [*Deamer and Kodama*, 1990]. Major impacts on the parent body may also cause short-term heating that remagnetize material near the impact site.

[81] Aqueous alteration in the nebular gas or on the planetesimal may further erode any preaccretional remanence. Several common magnetic phases found in chondrites (e.g.,

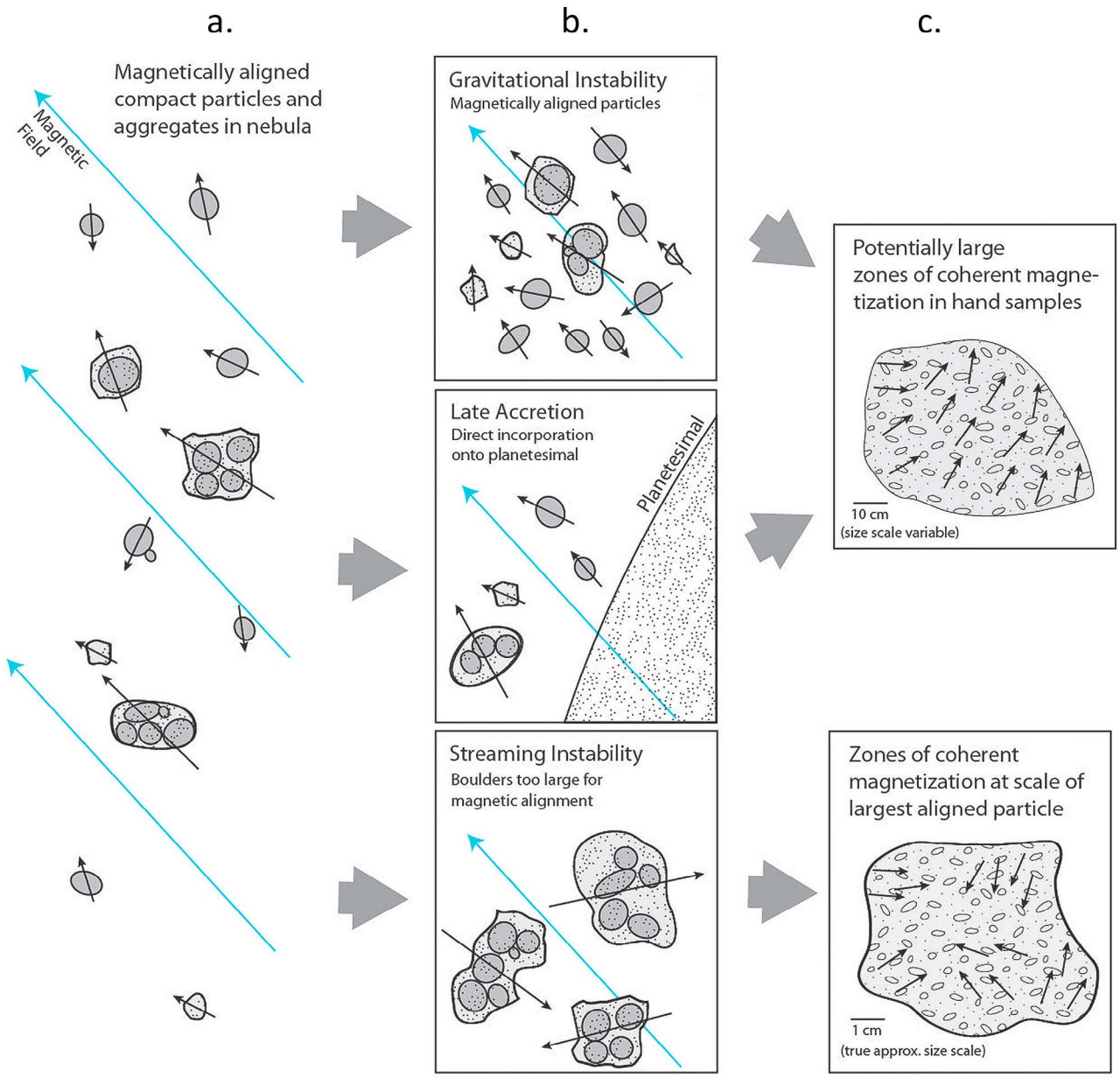

Figure 6. Three possible pathways for the accretionary growth of solid particles in the solar nebula and predicted ADRM zones. (a) Particles, including chondrules, CAIs, lithic clasts, and porous dust aggregates, grow or are formed in the size range in which magnetic alignment is active (up to several centimeters; see Figure 3). Magnetic moments of particles are shown by black arrows and background magnetic field is shown by blue arrows. (b, c) In the gravitational collapse scenario for small particles (Figure 6b (top) [*Cuzzi et al.*, 2008]), the gentle accretion of magnetically aligned particles may produce large (tens of centimeter or larger) ADRM zones in hand samples (Figure 6c, top). Late accretion of aligned particles onto planetesimals may produce the same result (Figure 6b, middle). On the other hand, streaming instabilities (Figure 6c (bottom) [*Johansen et al.*, 2007]) require larger boulders that have already outgrown the size range of magnetic alignment, resulting in final ADRM zones no larger than the maximum size of magnetic alignment (typically centimeter-sized). In this case the ADRM zones formed when the particles and agglomerates were incorporated into the boulders before onset of the streaming instability.

magnetite, pyrrhotite, and Ni-rich Fe-Ni alloys) are suggestive of metasomatic activity, although it is not entirely clear whether this occurred before or after planetesimal accretion [*Brearley*, 2003]. Reheating in the nebula or due to thermal metamorphism on the planetesimal may also cause partial demagnetization and/or magnetic overprinting [*Carporzen et al.*, 2011], although metamorphic temperatures sufficient for complete demagnetization are not observed except for high petrologic type chondrites [*Scott*, 2007].

[82] In summary, the physics of small particle collisions and the origin and alteration of magnetic mineral phases in the solar nebula are not well-known, and the discussion above describes plausible scenarios where uniform magnetization in accreting particles may become preserved on a planetesimal object.

4.3. Stability of Background Magnetic Field

[83] The orientation and intensity of the magnetic field in the solar nebula can be changed by shear in the ionized gas medium and diffusive decay due to ohmic losses. Magnetic coherence of particles may be destroyed if the direction of the field changes faster than the timescale of magnetic grain rotation. The latter timescale is equal to t_{drag} instead of t_{align} (which includes the contribution from t_{prec}) because particles traveling from one region of uniform field into another do not need to spin down. The diffusive decay timescale of magnetic fields is controlled by the local gas conductivity, which requires a source of ionization energy, and the size and abundance of grains, which deionize the gas by acting as sites for charge recombination. Larger dust grains are less efficient at depleting gas ions than smaller grains. During all phases of the solar nebula, the surface layers of the gas disk are subject to ionization by cosmic ray bombardment, and the interior of the disk is also partly ionized due to radioactive decay of its constituents. Furthermore, in the initially hot solar nebula, thermal excitation is sufficient to produce similarly high ionization fractions within about 1 AU [*Stepinski*, 1992]. During the early stages of the nebula, the small characteristic size of dust grains (<1 μm) reduces the conductivity of the gas such that the disk within $\sim$20 AU of the sun is unable to sustain strong magnetic fields by the shear motion of the gas (i.e., it is magnetically inactive) [*Sano et al.*, 2000]. However, by the time dust grains have coagulated into the size range where ADRM is active (up to several cm), the dust-rich midplane outside of 5 AU is magnetically active. Furthermore, even the region within 5 AU may be magnetically active due to turbulent mixing of strong magnetic fields from near the surfaces of the disk [*Turner et al.*, 2007]. Magnetic fields in the midplane of the disk are expected to be stable on the order of the Keplerian orbital period [*Turner and Sano*, 2008], which is at least one order of magnitude greater than t_{drag} for all particles less than 10 cm in diameter at all radii less than 20 AU. Anticipated field strengths in the 1–5 AU zone range between 10^{-5} and 10^{-4} T, consistent with the lowest assumption of field strength made in the this work.

[84] Even in the presence of a time-invariant magnetic field, solid particles may simply move in and out of zones of uniform fields if the spatial extent of uniform fields is small. To address this possibility, we take the simple approach of comparing the characteristic length scale of uniform magnetic fields to the distance traversed by a particle relative to the gas in t_{drag}. We assume that solid particles travel through the gas at their systemic drift velocity. *Turner et al.* [2007] find that the magnetic field is mostly unidirectional on scales smaller than $\sim$1/4 the gas disk scale height with $R < 5$ AU. At these orbital radii, the length scale of homogeneous magnetic fields is much longer than the path traveled by particles smaller than 10 cm within their t_{drag}. We therefore find that variations of nebular magnetic fields in both time and space do not pose a challenge for magnetic alignment within 5 AU. However, coupling between the magnetic fields and turbulent gas is stronger in the outer disk and the size scale of the smallest features in the magnetic field may be much smaller than the gas disk scale height if R is much greater than 5 AU. Therefore, it is possible and small field domains can interfere with particle alignment within 20 AU, although the precise size scale of field heterogeneities has yet to be studied at these radii. The observation of ADRM in primitive materials would constrain the minimum size of magnetic field heterogeneities in the region of accretion.

4.4. Detection of ADRM

[85] Two methods for the detection of ADRM are available: paleomagnetic studies of samples of small bodies (meteorites and returned samples) and in situ magnetometry of small bodies. The following characteristics of ADRM may aid in its positive identification in both the laboratory and on small bodies:

[86] 1. Depending on the accretion scenario, ADRM may be manifested in meteorites as millimeter to centimeter-scale zones of uniform magnetization, with intermediate regions of suppressed magnetization formed by the scrambling of surface grain orientations upon accretionary impact (Figure 6c, top). Even larger zones of coherent magnetization may be observed depending on the nebular mechanisms for accretionary growth (i.e., Figure 6).

[87] 2. The ADRM component is likely to be blocked to the Curie temperatures (the temperature above which no remanent magnetization can exist for a given magnetic mineral) of the constituent magnetic minerals, although it may be unblocked at lower temperatures if individual grains in the sample have been subjected to a partial thermal remagnetization event prior to agglomeration.

[88] 3. Studies of terrestrial DRM, the intensity of ADRM magnetization is likely to be one to two orders of magnitude less efficient than TRM, possibly on the order of 10^{-4} of the saturation isothermal remanent magnetization of the same sample [*Stacey*, 1972].

[89] 4. Even if a slab of meteoritic material carries a bulk ADRM, the magnetic moments of individual components (chondrules, CAIs, lithic clasts) should not be precisely unidirectional; each would be misaligned from the net moment direction while the overall the magnetization would tend towards one direction. This stands in contrast to a TRM, which would produce well-aligned magnetizations down to much finer scales (within the limits of magnetic anisotropy within each component).

[90] 5. On unheated bodies such as comets, ADRM may be the most likely explanation for any detected remanence.

[91] ADRM may have already been observed in meteorite hand samples, although the available data are ambiguous. In a detailed study of the Abee enstatite chondrite, *Sugiura and Strangway* [1983] found that NRM directions from subsamples taken from a single $\sim$1 cm clast ("Clast C") fell into two groups, with each group corresponding to a distinct section of the clast. To explain this observation, the authors proposed a partial TRM event prior to accretion in which the clast was not uniformly heated, but the plausibility of a large temperature contrast on a one centimeter body is uncertain. In any case, Abee is estimated to have experienced peak metamorphic temperatures of $\sim 640^{\circ}$ C on the parent body, which should have limited preservation of magnetization acquired prior to and during accretion [*Fogel et al.*, 1989].

[92] A later study of 17 mutually oriented chondrules in the Allende CV carbonaceous chondrite identified clustering of magnetic moment orientations in a direction dissimilar from that of the matrix. The authors conjectured that the chondrules' coherent orientations may reflect "depositional or accretional remanence" [*Sugiura and Strangway*, 1985]. More recently, *Carporzen et al.* [2011] detected the existence of several distinct zones of remanence direction in the matrix of Allende. After removing a mid-temperature unidirectional overprint (the authors' "MT" component), high-temperature remanence (the "HT" magnetization) of adjacent subsamples generally showed concordant directions while subsamples taken with separations of several millimeters or greater showed distinct moment orientations. This HT magnetization might be a manifestation of ADRM, while the MT component cannot be an ADRM because it is only blocked up to 290 C (see Point 2 above). On the other hand, even the identification of the HT component as ADRM is suspect because Allende has been extensively metasomatized such that few ferromagnetic minerals present during accretion remain [*Carporzen et al.*, 2011].

[93] Despite these intriguing observations, no unambiguous detection of ADRM has been made in hand specimen. Further laboratory work is required for the positive identification and characterization of ADRM. This should consist of the mapping of remanent magnetization on the millimeter or greater scale in a range of meteorite groups. Characterization of blocking temperature, mineralogy, and local porosity will aid in ruling out CRM and inhomogeneous partial TRM as alternative sources of magnetic heterogeneity. Furthermore, the observation of demagnetized (i.e., "scrambled") zones between adjacent ADRM zones would argue strongly in favor of ADRM (Figure 6c, top). Observations of consistency between magnetization and accretional textures, such as uniform magnetization in the dusty rims of CM chondrules [*Metzler et al.*, 1992], would also provide strong evidence for ADRM.

[94] Strong net dipole moments may have been detected during spacecraft flybys of the asteroids Gaspra and Braille [*Kivelson et al.*, 1993; *Richter et al.*, 2001]. However, a large number of mutual non-unidirectional ADRM zones at the meter scale or smaller is unlikely to result in a strong net dipole when observed from an orbiting spacecraft. Magnetic zones of the sizes expected from ADRM can only be detected in situ by measurements directly on the surface of a body. Although no such remanent crustal fields was detected on the one asteroid surface that has been visited [*Acuña et al.*, 2002], in 2015 the Rosetta orbiter and Philae lander are scheduled to measure the magnetic field of comet 67P/Churyumov–Gerasimenko. Because comets have not been globally heated since their accretion, they should not have a TRM. Other alternatives for the origin of cometary remanence are isothermal remanent magnetization (IRM) acquired in a strong external field, shock remanent magnetization (SRM), and CRM. IRM requires a strong, stable field of presently unknown origin, while SRM should be highly localized near impact features. Furthermore, modern interplanetary fields (order 0.5 nT) are likely too weak to be recorded as SRM and CRM. As discussed in section 4.2, certain accretional histories such as gravitational instabilities and late accretion can potentially form large ADRM zones. The resulting magnetic fields may be detectable from a magnetometer such as the one onboard the Philae lander, which will make measurements $\sim$1 m above the comet's surface [*Auster et al.*, 2007; *Bibring et al.*, 2007; *Glassmeier et al.*, 2007].

4.5. Implications of ADRM

[95] What can observations of ADRM tell us about the accretional phase of the solar nebula? With respect to nebular structure, the detection of ADRM would set a lower bound on the size scale of magnetically coupled eddies, as ADRM requires that regions of uniform field be large enough such that particles passing through them can align to the field before they pass into another eddy.

[96] The identification of ADRM would represent the first unambiguous detection of magnetic remanence acquired in solar nebular magnetic fields. Its preservation would therefore constrain the intensity of nebular fields and the extent of subsequent demagnetization processes (e.g. recrystallization, thermal metamorphism, shock events) and overprinting episodes acting in the nebular gas and on the parent body. Coherence of magnetization on scales of larger than a few centimeters within a sample would provide evidence of formation via a quickly-accreting gravitational instability or thorough late accretion. It may be possible for a large fraction or even all of a planetesimal to be uniformly magnetized.

[97] The hypothetical detection of small ADRM zones on the centimeter scale or smaller would suggest that solids agglomerated past the maximum size of magnetic alignment before their incorporation into a planetesimal. This is consistent with a streaming instability scenario involve decimeter to meter-sized boulders or with incremental growth. In such cases, large scale coherence among ADRM zones may be due to rapid accretion of particles onto a parent body. The rate of accretion onto the parent body surface must be quick compared to the timescale of the parent body's rotation with respect to a background field. Alternatively, the presence of strong surface fields on the parent body, possibly due to an internal dynamo, may be able to align incoming particles quickly and lead to coherent orientations upon accretion.

[98] The size of ADRM zones would indicate that particles were aggregated to at least the size scale of the zones before final accretion. Therefore, observation of millimeter-centimeter scale zones suggests that particle agglomeration was possible at these size scales, despite high velocity collisions. As seen in Figure 3, the size of expected magnetic zones is rather insensitive to solar nebula location but is a strong function of particle shape, turbulent gas velocity, and background field strength. Given the similar effects of these three parameters, a precise estimate of ancient field intensity may remain elusive. On the other hand, the presence of ADRM provides a lower bound on the possible strength of solar nebula magnetic fields.

5. Conclusions

[99] In this work, we have introduced a theoretical framework to judge the plausibility of accretional detrital remanent magnetization (ADRM) and predict its possible manifestations in primitive solar system material. We have shown that ferromagnetic particles between $\sim 30\ \mu$m and several cm in size may align with the background field in the solar nebula and subsequently accrete to form ADRM, which is

potentially observable in primitive meteorites and small bodies. We have considered a series of processes that govern the efficiency of ADRM acquisition and estimated the particles sizes that are subject to forming ADRM. Factors that may interfere with particle alignment in the nebular gas include mutual particle collisions, rotational Brownian motion, aerodynamic torque, radiative torque, and magnetic field instability in time and space. Using plausible values for the magnetic field strength (>1 μT), rotational gas drag is not sufficient to hinder alignment within the timescale of successive particle collisions and in fact aids particle alignment by quickly damping random rotations of particles. This is distinct from DRM on Earth, where viscous drag prevents rapid alignment of larger particles. For most orbital radii $\lesssim$20 AU, rotational Brownian motion and aerodynamic torque provide the lower and upper size limits on particles that can be successfully aligned to the background field. Meanwhile, radiative torques play a significant role for small particles in the inner nebula ($\lesssim$1.5 AU). The necessary condition of temporal field stability appears to be satisfied for the solar nebular outside of about 2 AU and for all distances from the central plane. The size scale of magnetic field heterogeneity must not be small such that solid particles can traverse them faster than their alignment timescale.

[100] The upper size limit for magnetic alignment in the solar nebula (Figure 3) is $\sim$1000 times larger than that for terrestrial DRM. Magnetic particles within the size range of efficient alignment that accrete with another such particle will grow while maintaining their net magnetic moment until they reach the upper end of this size range. Gravitational instabilities or rapid accretion in a slowly changing field may lead to coherence among the magnetic orientations of accreted particles at larger scales of >1 m. Although the degree of preservation of grain orientations upon accretionary collision beyond this stage cannot be quantified, grain collision experiments suggest that a significant portion (>30%) of the projectile's material becomes compressed but is otherwise left intact. Further metasomatism and impacts on the planetesimal body may weaken the magnitude of the remanence, but a pathway by which the uniform magnetic remanence in nebular agglomerates may be preserved in larger bodies is established.

[101] Zones of unidirectional magnetization (Figure 6c, top and middle) may potentially be observed in primitive samples, such as chondritic matrices. These zones are likely separated by regions of low magnetic coherence among grains. Monolithic particles such as CAIs and chondrules may also show mutually coherent magnetic orientations, resembling those observed by *Sugiura and Strangway* [1985]. Along with CRM, ADRM represents a plausible origin for observed magnetic coherence on the millimeter to centimeter scale observed in some chondrites (e.g., the HT magnetization studied by *Carporzen et al.* [2011]). Other possible detections of ADRM in meteorite samples and by spacecraft measurements exist, but so far the interpretation of all of these observations as ADRM remains ambiguous.

[102] If detected, the characterization of ADRM would have important implications for the structure of the solar nebula turbulence, the nature of early magnetic fields, and the thermal, chemical, and impact history of primitive bodies. Furthermore, structure of ADRM zones would constrain the formation process of the sample, distinguishing between the various hypothesized accretion scenarios. ADRM zones could be identified by conducting detailed mapping of magnetization directions in primitive meteorite samples. A true ADRM may be distinguished from other forms of remanence by its characteristic larger-scale (centimeters or larger) non-unidirectionality, low intensity, and the fact that it is blocked up to the Curie temperature. ADRM may also be detected by spaceborne magnetometry measurements of small bodies such as comets and primitive asteroids. We hope that this work will encourage further experimental studies to detect this new form of remanent magnetization.

[103] **Acknowledgments.** We thank K.-H. Glassmeier, U. Auster, I. Richter, and E. Beitz at TU Braunschweig for fruitful discussions and three anonymous referees for thoughtful and detailed comments that significantly improved the manuscript. We thank T. Peterson and the NASA Origins program for financial support.

References

Acuña, M., B. Anderson, C. Russell, P. Wasilewski, G. Kletetshka, L. Zanetti, and N. Omidi (2002), Near magnetic field observations at 433 Eros: First measurements from the surface of an asteroid, *Icarus*, *155*, 220–228.

Anson, G., and K. Kodama (1987), Compaction-induced inclination shallowing of the post-depositional remanent magnetization in a synthetic sediment, *Geophys. J. R. Astron. Soc.*, *88*, 673–692.

Auster, H., et al. (2007), Romap: Rosetta magnetometer and plasma monitor, *Space Sci. Rev.*, *128*(1), 221–240.

Balbus, S., and J. Hawley (2000), Solar nebula magnetohydrodynamics, *Space Sci. Rev.*, *92*, 39–54.

Bibring, J., et al. (2007), The Rosetta lander ("Philae") investigations, *Space Sci. Rev.*, *128*(1), 205–220.

Bockelée-Morvan, D., D. Gautier, F. Hersant, J. Huré, and F. Robert (2002), Turbulent radial mixing in the solar nebula as the source of crystalline silicates in comets, *Astron. Astrophys.*, *384*, 1107–1118.

Bradley, J. (1994), Chemically anomalous, preaccretionally irradiated grains in interplanetary dust from comets, *Science*, *265*(5174), 925.

Brearley, A. (2003), Nebular versus parent-body processing, *Treatise Geochem.*, *1*, 247–268.

Carporzen, L., B. Weiss, L. Elkins-Tanton, D. Shuster, D. Ebel, and J. Gattacceca (2011), Magnetic evidence for a partially differentiated carbonaceous chondrite parent body, *Proc. Natl. Acad. Sci. U. S. A.*, *108*, 6386–6389.

Cazaux, S., P. Caselli, A. Tielens, J. Bourlot, and M. Walmsley (2005), Molecular hydrogen formation on grain surfaces, in *J. Phys. Conf. Ser.*, *6*, 155–160.

Chiang, E., and P. Goldreich (1997), Spectral energy distributions of T Tauri stars with passive circumstellar disks, *Astrophys. J.*, *490*, 368–376.

Cho, J., and A. Lazarian (2007), Grain alignment and polarized emission from magnetized T Tauri disks, *Astrophys. J.*, *669*, 1085–1097.

Collinson, D. (1965), Depositional remanent magnetization in sediments, *J. Geophys. Res.*, *70*, 4663–4668.

Cuzzi, J., and R. Hogan (2003), Blowing in the wind: I. velocities of chondrule-sized particles in a turbulent protoplanetary nebula, *Icarus*, *164*(1), 127–138.

Cuzzi, J., R. Hogan, and K. Shariff (2008), Toward planetesimals: Dense chondrule clumps in the protoplanetary nebula, *Astrophys. J.*, *687*, 1432–1447.

Davis, L., and J. Greenstein (1951), The polarization of starlight by aligned dust grains., *Astrophys. J.*, *114*, 206–240.

Deamer, G., and K. Kodama (1990), Compaction-induced inclination shallowing in synthetic and natural clay-rich sediments, *J. Geophys. Res.*, *95*, 4511–4529.

Dolginov, A., and I. Mytrophanov (1976), Orientation of cosmic dust grains, *Astrophys. Space Sci.*, *43*(2), 291–317.

Dominik, C., and H. Nübold (2002), Magnetic aggregation: dynamics and numerical modeling, *Icarus*, *157*, 173–186.

Draine, B., and J. Weingartner (1996), Radiative torques on interstellar grains. I. Superthermal spin-up, *Astrophys. J.*, *470*, 551–565.

Draine, B., and J. Weingartner (1997), Radiative torques on interstellar grains. II. Grain alignment, *Astrophys. J.*, *480*, 633–646.

Dubrulle, B., G. Morfill, and M. Sterzik (1995), The dust subdisk in the protoplanetary nebula, *Icarus*, *114*, 237–246.

Fogel, R., P. Hess, and M. Rutherford (1989), Intensive parameters of enstatite chondrite metamorphism, *Geochim. Cosmochim. Acta*, *53*, 2735–2746.

Galdi, G., and A. Vaidya (2001), Translational steady fall of symmetric bodies in a Navier–Stokes liquid, with application to particle sedimentation, *J. Math. Fluid Mech.*, *3*, 183–211.

Glassgold, A., R. Meijerink, and J. Najita (2009), Formation of water in the warm atmospheres of protoplanetary disks, *Astrophys. J.*, *701*, 142–153.

Glassmeier, K., H. Boehnhardt, D. Koschny, E. Kührt, and I. Richter (2007), The Rosetta mission: Flying towards the origin of the solar system, *Space Sci. Rev.*, *128*(1), 1–21.

Gold, T. (1952), The alignment of galactic dust, *Mon. Not. R. Astron. Soc.*, *112*, 215–218.

Güttler, C., J. Blum, A. Zsom, C. Ormel, and C. Dullemond (2010), The outcome of protoplanetary dust growth: Pebbles, boulders, or planetesimals?, *Astron. Astrophys.*, *513*, A56.

Hayashi, C. (1981), Structure of the solar nebula, growth and decay of magnetic fields and effects of magnetic and turbulent viscosities on the nebula, *Suppl. Progress Theor. Phys.*, *70*, 35–53.

Heslop, D. (2007), Are hydrodynamic shape effects important when modelling the formation of depositional remanent magnetization?, *Geophys. J. Int.*, *171*, 1029–1035.

Hollenbach, D., and E. Salpeter (1971), Surface recombination of hydrogen molecules, *Astrophys. J.*, *163*, 155–164.

Ivanov, S., and A. Yanshin (1980), Forces and moments acting on bodies rotating about a symmetry axis in a free molecular flow, *Fluid Dyn.*, *15*, 449–453.

Johansen, A., J. Oishi, M. Mac Low, H. Klahr, and T. Henning (2007), Rapid planetesimal formation in turbulent circumstellar disks, *Nature*, *448*(7157), 1022–1025, doi:10.1038/nature06086.

Joung, M., M. Mac Low, and D. Ebel (2004), Chondrule formation and protoplanetary disk heating by current sheets in nonideal magnetohydrodynamic turbulence, *Astrophys. J.*, *606*, 532–541.

Kivelson, M., L. Bargatze, K. Khurana, D. Southwood, R. Walker, and P. Coleman (1993), Magnetic field signatures near galileo's closest approach to gaspra, *Science*, *261*, 331–334.

Lazarian, A. (2007), Tracing magnetic fields with aligned grains, *J. Quant. Spectrosc. Radiat. Transfer*, *106*, 225–256.

Lazarian, A., and T. Hoang (2007), Radiative torques: analytical model and basic properties, *Mon. Not. R. Astron. Soc.*, *378*, 910–946.

Lazarian, A., and T. Hoang (2008), Alignment of dust with magnetic inclusions: radiative torques and superparamagnetic Barnett and nuclear relaxation, *Astrophys. J. Lett.*, *676*, L25.

Levy, E., and S. Araki (1989), Magnetic reconnection flares in the protoplanetary nebula and the possible origin of meteorite chondrules, *Icarus*, *81*, 74–91.

Lord, R. (1964), The aerodynamic resistance to a rotating sphere in the transition regime between free molecule and continuum creep flow, *Proc. R. Soc. London, Ser. A*, *279*, 39–49.

McNown, J., and J. Malaika (1950), Effects of particle shape on settling velocity at low reynolds numbers, *Eos Trans. AGU*, *31*, 74–82.

Metzler, K., A. Bischoff, and D. Stöffler (1992), Accretionary dust mantles in CM chondrites: Evidence for solar nebula processes, *Geochim. Cosmochim. Acta*, *56*, 2873–2897.

Nakagawa, Y., M. Sekiya, and C. Hayashi (1986), Settling and growth of dust particles in a laminar phase of a low-mass solar nebula, *Icarus*, *67*, 375–390.

Nakamura, T., et al. (2008), Chondrulelike objects in short-period comet 81p/wild 2, *Science*, *321*(5896), 1664.

Nübold, H., and K. Glassmeier (2000), Accretional remanence of magnetized dust in the solar nebula, *Icarus*, *144*, 149–159.

Nübold, H., T. Poppe, M. Rost, C. Dominik, and K. Glassmeier (2003), Magnetic aggregation: II. Laboratory and microgravity experiments, *Icarus*, *165*, 195–214.

Ormel, C., J. Cuzzi, and A. Tielens (2008), Co-accretion of chondrules and dust in the solar nebula, *Astrophys. J.*, *679*, 1588–1610.

Paraskov, G., G. Wurm, and O. Krauss (2007), Impacts into weak dust targets under microgravity and the formation of planetesimals, *Icarus*, *191*, 779–789.

Purcell, E. (1979), Suprathermal rotation of interstellar grains, *Astrophys. J.*, *231*, 404–416.

Richter, I., D. Brinza, M. Cassel, K. Glassmeier, F. Kuhnke, G. Musmann, C. Othmer, K. Schwingenschuh, and B. Tsurutani (2001), First direct magnetic field measurements of an asteroidal magnetic field: DS1 at Braille, *Geophys. Res. Lett.*, *28*, 1913–1916.

Sano, T., M. Shoken, T. Umebayashi, and T. Nakano (2000), Magnetorotational instability in protplanetary disks. II. Ionization state and unstable regions, *Astrophys. J.*, *543*, 486–501.

Scott, E. (2007), Chondrites and the protoplanetary disk, *Annu. Rev. Earth Planet. Sci.*, *35*, 577–620.

Spitzer, L., and J. Tukey (1951), A theory of interstellar polarization, *Astrophys. J.*, *114*, 187–205.

Stacey, F. (1972), On the role of brownian motion in the control of detrital remanent magnetization of sediments, *Pure Appl. Geophys.*, *98*(1), 139–145.

Stepinski, T. (1992), Generation of dynamo magnetic fields in the primordial solar nebula, *Icarus*, *97*, 130–141.

Sugiura, N., and D. Strangway (1983), A paleomagnetic conglomerate test using the Abee E4 meteorite, *Earth Planet. Sci. Lett.*, *62*, 169–179.

Sugiura, N., and D. Strangway (1985), NRM directions around a centimeter-sized dark inclusion in Allende, *Proc. Lunar Planet. Sci. Conf., 15th*, Part 2, *J. Geophys. Res.*, *90*, suppl., C729–C738.

Tauxe, L., J. Steindorf, and A. Harris (2006), Depositional remanent magnetization: Toward an improved theoretical and experimental foundation, *Earth Planet. Sci. Lett.*, *244*, 515–529.

Taylor, J. (2005), *Classical Mechanics*, pp. 173–179, Univ. Sci. Books, Herndon, Va.

Teiser, J., and G. Wurm (2009), High-velocity dust collisions: Forming planetesimals in a fragmentation cascade with final accretion, *Mon. Not. R. Astron. Soc.*, *393*, 1584–1594.

Tsuchiyama, A., R. Shigeyoshi, T. Kawabata, T. Nakano, K. Uesugi, and S. Shirono (2003), Three-dimensional structures of chondrules and their high-speed rotation, *Lunar Planet. Sci.*, *XXXIV*, Abstract 1271.

Turner, N., and T. Sano (2008), Dead zone accretion flows in protostellar disks, *Astrophys. J. Lett.*, *679*, L131–L134.

Turner, N., T. Sano, and N. Dziourkevitch (2007), Turbulent mixing and the dead zone in protostellar disks, *Astrophys. J.*, *659*, 729–737.

Wang, M., Q. Chen, and Q. Ding (2010), Synthesis of SiO_2 spheres with magnetic cores: Implications for the primary accretion in the solar nebula, *J. Geophys. Res.*, *115*, E05005, doi:10.1029/2009JE003412.

Wardle, M. (2007), Magnetic fields in protoplanetary disks, *Astrophys. Space Sci.*, *311*, 35–45.

Weidenschilling, S. (1977), Aerodynamics of solid bodies in the solar nebula, *Mon. Not. R. Astron. Soc.*, *180*, 57–70.

Weidenschilling, S. (1984), Evolution of grains in a turbulent solar nebula, *Icarus*, *60*, 553–567.

Weidenschilling, S., and J. Cuzzi (2006), Accretion dynamics and timescales: Relation to chondrites, in *Meteorites and the Early Solar System II*, edited by D. S. Lauretta and H. McSween, pp. 473–485, Univ. of Ariz., Tucson.

Weiss, B., J. Berdahl, L. Elkins-Tanton, S. Stanley, E. Lima, and L. Carporzen (2008), Magnetism on the angrite parent body and the early differentiation of planetesimals, *Science*, *322*, 713–716.

Weiss, B., J. Gattacceca, S. Stanley, P. Rochette, and U. Christensen (2010), Paleomagnetic records of meteorites and early planetesimal differentiation, *Space Sci. Rev.*, *152*, 341–390.

Willacy, K., H. Klahr, T. Millar, and T. Henning (1998), Gas and grain chemistry in a protoplanetary disk, *Astron. Astrophys.*, *338*, 995–1005.

Wurm, G., G. Paraskov, and O. Krauss (2005), Growth of planetesimals by impacts at 25 m/s, *Icarus*, *178*, 253–263.

Zolensky, M., et al. (2006), Mineralogy and petrology of comet 81p/Wild 2 nucleus samples, *Science*, *314*, 1735–1739.

Zsom, A., C. Ormel, C. Güttler, J. Blum, and C. Dullemond (2010), The outcome of protoplanetary dust growth: pebbles, boulders, or planetesimals? II. Introducing the bouncing barrier, *Astron. Astrophys.*, *513*, A57.

R. R. Fu and B. P. Weiss, Department of Earth, Atmospheric and Planetary Sciences, Massachusetts Institute of Technology, 77 Massachusetts Ave., Cambridge, MA 02139, USA. (rogerfu@mit.edu)